Current Biology

ARSK1 activates TORC1 signaling to adjust growth to phosphate availability in Arabidopsis

--Manuscript Draft--

Manuscript Number:	CURRENT-BIOLOGY-D-22-01893R2
Full Title:	ARSK1 activates TORC1 signaling to adjust growth to phosphate availability in Arabidopsis
Article Type:	Report
Corresponding Author:	Hatem Rouached East Lansing, UNITED STATES
First Author:	Huikyong Cho
Order of Authors:	Huikyong Cho
	Michael Banf
	Zaigham Shahzad
	Jelle Van Leene
	Flavia Bossi
	Sandrine Ruffel
	Nadia Bouain
	Pengfei Cao
	Gabiel Krouk
	Geert De Jaeger
	Benoit Lacombe
	Federica Brandizzi
	Seung Y. Rhee
	Hatem Rouached
Abstract:	Nutrient sensing and signaling are essential for adjusting growth and development to available resources. Deprivation of the essential mineral phosphorus (P) inhibits root growth. The molecular processes that sense P limitation to trigger early root growth inhibition are not known yet. Target of rapamycin (TOR) kinase is a central regulatory hub in eukaryotes to adapt growth to internal and external nutritional cues. How nutritional signals are transduced to TOR to control plant growth remains unclear. Here, we identify Arabidopsis Root Specific Kinase 1 (ARSK1) which attenuates initial root growth inhibition in response to P limitation. We demonstrate that ARSK1 phosphorylates and stabilizes the Regulatory-Associated Protein of TOR 1B (RAPTOR1B), a component of the TOR complex 1, to adjust root growth to P availability. These findings uncover signaling components acting upstream of TOR to balance growth to P availability.
Additional Information:	
Question	**Response**
Standardized datasets A list of datatypes considered standardized under Cell Press policy is available here. Does this manuscript report new standardized datasets?	No

Original Code Does this manuscript report original code?	No

ARSK1 activates TORC1 signaling to adjust growth to phosphate availability in Arabidopsis

Huikyong Cho[1,2], Michael Banf[3], Zaigham Shahzad[4], Jelle Van Leene[5,6], Flavia Bossi[3], Sandrine Ruffel[7], Nadia Bouain[7], Pengfei Cao[8], Gabiel Krouk[7], Geert De Jaeger[5,6], Benoit Lacombe[7], Federica Brandizzi[8], Seung Y. Rhee[3,*], Hatem Rouached[1,2,9,*]

1-The Plant Resilience Institute, Michigan State University, MI 48824, USA
2-Department of Plant, Soil, and Microbial Sciences, Michigan State University, MI 48824, USA
3-Department of Plant Biology, Carnegie Institution for Science, Stanford, CA 94305, USA
4-Department of Life Sciences, Lahore University of Management Sciences, Lahore 54792, Pakistan.
5-Ghent University, Department of Plant Biotechnology and Bioinformatics, 9052 Ghent, Belgium
6-VIB Center for Plant Systems Biology, 9052 Ghent, Belgium
7-Institute for Plant Sciences of Montpellier, Univ Montpellier, CNRS, INRAE, Montpellier 34060, France
8-MSU DOE-Plant Research Laboratory, Michigan State University, East Lansing Michigan, 48824 USA

[9]Leads Contact

*Correspondence: rouached@msu.edu (H.R.), srhee@carnegiescience.edu (S.Y.R); Twitter: @hatemrouached , @SueRhee2

Keywords

Root growth; Phosphorus deficiency; ARSK1, RAPTOR1B; TORC1 signaling; Arabidopsis

SUMMARY

Nutrient sensing and signaling are essential for adjusting growth and development to available resources. Deprivation of the essential mineral phosphorus (P) inhibits root growth[1]. The molecular processes that sense P limitation to trigger early root growth inhibition are not known yet. Target of rapamycin (TOR) kinase is a central regulatory hub in eukaryotes to adapt growth to internal and external nutritional cues[2,3]. How nutritional signals are transduced to TOR to control plant growth remains unclear. Here, we identify Arabidopsis Root Specific Kinase 1 (ARSK1) which attenuates initial root growth inhibition in response to P limitation. We demonstrate that ARSK1 phosphorylates and stabilizes the Regulatory-Associated Protein of TOR 1B (RAPTOR1B), a component of the TOR complex 1, to adjust root growth to P availability. These findings uncover signaling components acting upstream of TOR to balance growth to P availability.

RESULTS AND DISCUSSION

Target of rapamycin (TOR)[4] is a widely conserved serine/threonine protein kinase that integrates nutritional, growth, and stress signals to adjust growth in eukaryotes[2,3]. TOR operates in at least two multi-protein complexes (TORC1 and TORC2), though no evidence exists for TORC2 presence in plants[5,6]. The TORC1 complex comprises the conserved Regulatory-Associated Protein of TOR (RAPTOR) and the Lethal with Sec 13 (LST8) proteins[5,6]. RAPTOR acts as a scaffold to recruit substrate proteins to TOR for phosphorylation[5,6]. TORC1 activity is modulated by exogenous and endogenous signals such as light, hormones, energy deprivation, and nutrients[7,8]. While much is known about how TOR regulates cellular growth in response to environmental changes, molecular processes that modulate TOR activity remain poorly understood[9–11]. In plants, light and energy deprivation signals influence the activity of TORC1 through phosphorylation of RAPTOR1B by SnRK1 and SnRK2 kinase proteins[12–14]. Alternatively, light signals can activate TOR via GTPase ROP2[15]. The regulatory components used to balance nutrient deficiency stress response and growth through TOR pathway remain elusive.

Phosphorus (P) is an essential nutrient for plant growth and development as a key component of energy sources (ATP, ADP), nucleic acids (DNA, RNA) and membranes (phospholipids)[16]. Plants acquire P from soil through their roots[17]. Current agricultural practices require P fertilization, causing the worldwide P reserves to become increasingly scarce, and a potential P crisis looms for agriculture by the end of the 21st century[18–19]. Therefore, understanding how plants adjust growth to P availability is important to develop P use-efficient crops[20]. Although recognized as a central growth machinery in plants, whether and how TORC1 monitors P status in vascular plants to control growth remains unknown. Here, we used a combination of gene regulatory network inference, genetics, and biochemistry to discover regulatory components influencing TOR activity to control plant root growth in response to P availability.

P deficiency (-P) arrests primary root growth in the *Arabidopsis thaliana* reference ecotype Columbia (Col-0), which is hypothesized to be due to the accumulation of toxic levels of iron (Fe) in root tips[21]. However, primary root growth inhibition in response to P deprivation precedes alterations in Fe accumulation[22,23]. To confirm whether changes in Fe accumulation occur before root growth retardation, we investigated the effects of P limitation on Fe levels in root tips and root growth at early hours (3h, 6h, and 9h) after transfer to P deficient medium. We found a decrease in root growth without a change in Fe levels, indicating initial inhibition root growth by P deficiency is independent of alterations in Fe accumulation in the root tips (Figures 1A and 1B). Previously, no change in Fe levels was observed in root tips even at 24h under -P conditions, which concurs with the lack of change in the expression of Fe-uptake

transporters[21,22]. Therefore, the mechanism that senses external P availability to trigger growth inhibition in P deprived roots remains unknown.

To reveal early signaling processes mediating physiological responses to P availability, we performed global gene expression analysis of Col-0 roots exposed to different P regimes (+P and -P) for 3, 6, and 9 hours. Given the established interaction between P and Fe homeostasis in plants[21], Fe availability was also altered to identify transcriptional responses specific to P deprivation. Differentially expressed genes in at least one condition were used, in combination with further root-specific expression data as well as promoter binding information, to infer a putative gene regulatory network (GRN) architecture to identify key genes mediating early transcriptional responses to P availability (Figure 1C, Sup Table S1). The inferred GRN entailed 12 highly connected transcription factors (TFs): AT1G77200 (*ERF37*), AT1G15580 (*IAA5*), AT3G16280 (*ERF36*), AT3G56980 (*ORG3*), AT5G07700 (*MYB76*), AT4G17900 (*PLATZ11*), AT5G61430 (*NAC100*), AT5G54230 (*MYB49*), AT4G17490 (*ERF6*), AT4G28790 (*CITF2*), AT4G35770 (*SEN1*) and AT5G65640 (*bHLH093*) (Figure 1C). Intriguingly, our GRN analysis revealed that five of these TFs (*ERF36, ERF37, IAA5, MYB49, bHLH093*) had a common target: *ARABIDOPSIS ROOT SPECIFIC KINASE 1* (*ARSK1*, AT2G26290).

ARSK1 encodes a receptor-like kinase (RLK), which belongs to a large plant-specific family with members controlling diverse processes such as innate immunity and development of endodermal barriers, the Casparian strips[24–26]. ARSK1 belongs to a subfamily named RLCK VII-6[26], which includes RPM1-induced protein kinase (RIPK) that forms a receptor complex with FERONIA[11] to inhibit root growth in response to a peptide hormone RALF1[27]. *ARSK1* is mainly expressed in roots (Figure S1A) and repressed by P deprivation (Figure 1D). To assess the impact of ARSK1 on root growth response to P deficiency, we characterized mutant lines carrying a null allele *arsk1* (*arsk1-1* and *arsk1-2*) and *ARSK1* overexpressing (*ARSK1*-OE) lines (Figure S1B). In contrast to +P conditions, under -P conditions, primary roots of *arsk1-1* and *arsk1-2* mutant plants were significantly shorter than wild-type roots (Figures 1E, 1F, S1C). In contrast, *ARSK1*-OE root growth was not inhibited by -P (Figures 1E and 1F). Notably, the phenotype of *ARSK1* overexpressing lines is similar to the extensively studied *lpr1;lpr2* mutant, which maintains root growth under P deficiency[28,29]. LPR1 and LPR2 influence growth in P deprived roots through effects on Fe accumulation in root meristem and elongation zone[22]. Analysis of temporal response of root growth of *lpr1;lpr2*, *ARSK1*-OE, and Col-0 to P deficiency revealed a significant decrease in root growth of wild-type Col-0 as well as *lpr1;lpr2* mutant after 9h of P deficiency (Figure S1D). However, *ARSK1*-OE lines displayed no decrease in root growth after 9h of -P (Figure S1D). Moreover, to understand whether *arsk1* roots are shorter than WT under -P conditions due a change in root meristem length and/or a

change in cell elongation, we phenotyped WT, *arsk1* mutant for these traits (Figures S1E and S1F). Our results revealed that *arsk1* roots are shorter than Col-0 in -P because of a reduction in epidermal cell length (Figure S1F). These results demonstrate a role of ARSK1 in early root growth inhibition by -P. Furthermore, assessment of the relative expression level of *ARSK1* in the roots of wild-type plants (Col-0), *lpr1;lpr2*, and *aluminum-activated malate efflux transporter* (*almt1*) and the *histidine-2-cysteine-2 zinc finger stop1* mutants which also display longer root under -P[21,22] show that *ARSK1* was significantly downregulated by -P regardless of the genetic background (Figure S1G). Therefore, ARSK1 is a key component of a new molecular pathway controlling root growth in a P-dependent manner.

Next, we set out to study how ARSK1 could influence root growth response to -P. To identify putative partners of ARSK1, we first investigated the published *Arabidopsis* interactome[30]. In this high-throughput yeast-two hybrid (Y2H) screen, ARSK1 interacts with only RAPTOR1B, which is a scaffold protein of the TOR complex. Using targeted Y2H, we confirmed that ARSK1 indeed interacts with RAPTOR1B (Figure 2A). Gene expression analysis using qRT-PCR uncovered that *ARSK1* does not influence the expression of *RAPTOR1B*, and the expression of later is neither regulated by P availability nor by the above-mentioned genes including *LPR1*, *LPR2*, *ALMT1,* and *STOP1* (Figures S1G and S2A). To test whether ARSK1 and RAPTOR1B are coexpressed, we analyzed spatial expression patterns of these two genes using promoter::GUS fusion lines, as well as published transcriptome data across cells[31], tissues, and treatments[32]. Promoter::GUS fusion revealed that ARSK1 and RAPTOR1B are expressed in roots (Figures S1A and S2B), indicating that both promoters are active within the same organ. Analysis of published expression data in different root cell types revealed an overlap between *ARSK1 and RAPTOR1B* expression (Figure S2C). The co-expression of *ARSK1* and *RAPTOR1B* was further corroborated by a highly significant correlation ($p<0.00001$) across tissues and treatments (Figure S2D). Finally, to get an answer on whether the ARSK1 and RAPTOR have or share the same subcellular localization, we co-infiltrated *Nicotiana Benthamiana* leaves with i) RAPTOR1B tagged with GFP, and cytosolic mCherry (Figure S2E), and ii) ARSK1 tagged with GFP and cytosolic mCherry (Figure S2D). Our live-cell confocal microscopy observations confirmed that RAPTOR1B is mainly cytosolic, which is in line with early studies showing a cytosolic location of RAPTOR1B[13]. Our results show that both proteins, ARSK1 and RAPTOR1B, localize in the cytosol, while we cannot exclude other possible subcellular locations for ARSK1 (Figure S2E). Given that ARSK1 is a protein kinase, we investigated whether ARSK1 could phosphorylate RAPTOR1B. For this, we performed in vitro kinase assays using recombinant ARSK1 (Figure S3A) and RAPTOR1B purified from Arabidopsis PSB-d cell cultures through the N- or C-terminal GS^{rhino} tag (Figure 2B). These assays showed specific phosphorylation of RAPTOR1B by ARSK1 (Figure 2B). To identify

which residues of RAPTOR1B were phosphorylated, we repeated the kinase assay and identified phosphopeptides through mass spectrometry (Figure 2C). This analysis showed that ARSK1 can specifically phosphorylate two RAPTOR1B peptides. The first peptide contains three serine (S) residues (S^{739}, S^{740} or S^{741}) as putative phosphorylation sites, and the second peptide harbors S^{757} or threonine (T^{759}) (Figure 2C). Our results indicate that ARSK1 interacts with and phosphorylates RAPTOR1B (Figure 2**,** Table S3).

To assess whether RAPTOR1B affects root growth response to P limitation, we characterized *raptor1b* mutant plants grown in P-sufficient and P-deficient environments. The *raptor1b* mutant plants displayed significantly shorter primary roots than WT plants under -P and +P conditions. The *raptor1b* mutant phenocopies the *arsk1* mutant under -P (Figures 1E, 1F, 3A, 3B, and S3B). Next, to examine whether ARSK1 and RAPTOR1B mediate root growth response to P limitation through the same genetic pathway, we analyzed root growth of an a*rsk1-1;raptor1b* double mutant under different P regimes. We found that *arsk1-1;raptor1b* displays similar root growth under -P to that of *raptor1b* or *arsk1-1* single mutants (Figure 3C), indicating that ARSK1 and RAPTOR1B influence root growth in -P through the same genetic pathway. Moreover, to study the effects of RAPTOR1B phosphorylation on growth of P-deprived roots, we expressed phospho-mimicking (replacing S or T with aspartate (D)) and phospho-deficient (replacing S or T with alanine (A)) forms of RAPTOR1B for each of the putative phosphosites (S^{739}, S^{740}, S^{741}, S^{757}, or T^{759}) in *raptor1b* and *arsk1-1;raptor1b* mutant backgrounds (Figures 3D, S3B). The expression of only the S^{740} phospho-mimicking RAPTOR1B form (RAPTOR1BS^{740}D) alleviated root growth inhibition by -P in these mutants (Figure 3D), and complement the *raptor1b* root growth in +P conditions (Figure S3B). To assess the functional importance of RAPTOR1B Ser^{740} phosphorylation, we assessed RAPTOR1B protein abundance in Col-0, *arsk1-1* mutant, and *ARSK1-OE1*, RAPTOR1BS^{740}D and RAPTOR1BS^{740}A lines (Figures 4A and S3C**).** Under P sufficient conditions, we found higher levels of RAPTOR1B protein in RAPTOR1BS^{740}D and *ARSK1-OE* lines by comparison to Col-0, *arsk1-1*, and RAPTOR1BS^{740}A lines (Figure 4A). Furthermore, -P caused significant reduction in RAPTOR1B protein levels in Col-0, *arsk1*, and RAPTOR1BS^{740}A lines, and this reduction was remarkably extenuated in RAPTOR1BS^{740}D and *ARSK1-OE1* (Figure 4A). Taken together, our results show that ARSK1 mediates RAPTOR1B's S^{740} phosphorylation in a P-dependent manner that adjusts root growth to P availability.

Because -P represses *ARSK1* which phosphorylates a core component of TORC1, our biochemical and genetic experiments suggest that -P stress inhibits TORC1, thereby restricting root growth. To test this hypothesis, we examined the effect of a TOR inhibitor, AZD-8055, on root growth response to P deficiency as well as profiled TOR activity under P sufficient and deficient conditions[33–36]. AZD-8055 treatment resulted in a strong reduction of

root growth in WT plants in P-sufficient as well as P-deficient conditions (Figures 4B and S3D). Therefore, AZD8055 inhibits the root growth of *arsk1-1* and *raptor1b* mutants and WT to a similar level under P sufficient conditions. In contrast, neither *raptor1b* nor *arsk1-1* mutant plants responded to AZD-8055 treatment when grown in -P conditions (Figures 4C and S3D). Furthermore, analysis of TOR activity using plant S6 kinase (S6-K)[37,38] phosphorylation assays revealed that P deficiency remarkably decreased S6-K phosphorylation (S6K-p), indicating significantly reduced TOR activity in P-deprived roots (Figure 4D). Interestingly, overexpression of *ARSK1 (ARSK1-OE)* or *RAPTOR1BS^{740}D* prevented the decrease of S6K-p accumulation compared to Col-0 plants grown under P-deficient conditions (Figure 4D). Overall, our results support a central role of TORC1 and ARSK1 in root growth response to P availability and validate the premises of our working model for an ARSK1-TORC1 axis to maintain root growth in -P conditions.

Although several proteins are known to control the inhibition of primary root growth under P deficiency conditions in Arabidopsis[39], the factors affecting root response to early P deficiency have remained elusive. We discover a molecular module (ARSK1-RAPTOR1B) that integrates P availability cues with TOR signaling to control root growth within hours of P deficiency. While availability of nutrients, such as sulfur, influence plant growth via glucose-TOR signaling[40], our study shows that the inhibition of root growth response to -P is not dependent upon sucrose availability (Figure S3E), which is in line with previous reports[41]. Mechanistically, under P sufficient environments, ARSK1 protein phosphorylates RAPTOR1B, and the phosphorylated RAPTOR1B promotes TOR activity to maintain root growth (Figure 4E). In the absence of ARSK1, RAPTOR1B is not phosphorylated, which causes a reduction of its abundance, and therefore TOR activity is reduced, leading to the inhibition of root growth (Figure 4E). Therefore, our findings uncover a novel pathway that integrates P availability with the energy sensing TOR pathway. This discovery offers a new perspective on how to improve plant growth under P limitation through optimizing nutrient foraging by roots, which will become increasingly important for stewarding in sustainable agriculture. Moreover, our findings enable new avenues of investigation for seeking what senses the P status to relay the signal to ARSK1-RAPTOR1B-TOR, and what are the key metabolic and catabolic processes acting downstream TOR to regulate root growth[42].

ACKNOWLEDGMENTS

We thank Daniel J. Kliebenstein and Meike Burow for providing Arabidopsis *raptor1b* mutant seeds. This work was funded in part by the “Institut National de la Recherche Agronomique – Montpellier – France” INRA, the AgreenSkills Plus, The Plant Resilience Institute, and

Michigan State University (USA) to H.R., the Alexander von Humboldt Foundation (Postdoctoral Fellowship) to M.B, the National Institutes of Health grant R35 GM136637 to F.B., the U.S. National Science Foundation grants MCB-1617020, IOS-1546838, and the Water and Life Interface Institute (WALII) DBI grant # 2213983 and the U.S. Department of Energy, Office of Science, Office of Biological and Environmental Research, Genomic Science Program grant nos. DE-SC0018277, DE-SC0008769, DE-SC0020366 and DE-SC0021286 to SYR. Z.S. was supported by FIF-781-BIO and CRP/PAK22-05_EC through ICGEB. This work was done in part on the ancestral land of the Muwekma Ohlone Tribe, which was and continues to be of great importance to the Ohlone people. The funders had no role in study design, data collection and analysis, decision to publish, or preparation of the manuscript.

AUTHOR CONTRIBUTIONS

Conceptualization, H.R., S.Y.R., Z.S.; Methodology, G.B., S.J.U., V.R., D.S., E.S., N.S., F.L.S., R.D.M., and R.D.I.; Formal Analysis, H.C., N.B., S.R., B.L., M.B., F.B., J.V.L., and G.D.J, and P.C.; Investigation, H.C., N.B., S.R., B.L., M.B., F.B., J.V.L., and G.D.J, and P.C., and H.R.,; Data Curation, H.C., N.B., S.R., B.L., and F.B.; Writing– Original Draft Preparation, H.R., S.Y.R., Z.S, and F.B.; Writing– Review & Editing, H.R., S.Y.R., Z.S, and F.B.; Supervision, H.R.; Project Administration, H.R.; Funding Acquisition, H.R., S.Y.R., Z.S., and F.B.

DECLARATION OF INTERESTS

The authors declare no competing interests.

FIGURE LEGENDS.

Figure 1. ARSK1 mediates the inhibition of early root growth by phosphorus (P) deficiency.

A) WT seedlings grown under +Pi for 5 days were transferred to +Pi or −Pi medium for 3, 6, and 9 h. Average (±95% confidence interval) change in Col-0 primary root length for 9 hours after transfer of seedlings to P-deficient conditions. Δ measure indicates the difference in root length after transfer to -P versus +P. Data shown are from 3 experiments, each experiment with 10 plants. The letters represent statistically different means at $p < 0.05$ (one-way ANOVA with a Duncan post hoc test).

B) WT seedlings grown under +Pi for 5 days were transferred to +Pi or −Pi medium for 3, 6, and 9 h. Average (±95% confidence interval) Fe concentrations in primary root tips of Col-0 for 9 hours after transfer to P-deficient conditions. Data shown are from 3 experiments, each

experiment with 10 plants. The letters represent statistically different means at $p < 0.05$ (one-way ANOVA with a Duncan post hoc test).

C) Inferred regulatory network of genes responsive to -P (light blue), -Fe (red), and -P and -Fe (dark blue) deficiency. Responsiveness to multiple conditions per gene is colored as -P+Fe and +P-Fe (green), -P+Fe and -P-Fe (orange), +P-Fe and -P-Fe (violet) as well as -P+Fe and +P-Fe and -P-Fe (brown). Analogous coloring of arrows between genes indicates inferred condition specificity of gene regulation between transcription factors (circles) and putative targets (rectangles). The gene identifiers of the transcription factors and the *ARABIDOPSIS ROOT SPECIFIC KINASE* (*ARSK1*) gene (triangle) are indicated as black dashed lines.

D) Mean *ARSK1* mRNA abundance relative to Ubiquitin 10 in the roots of Col-0 grown in the presence of +P for 7 days and transferred to +P or -P for 6 h. Data shown from 3 biological repeats. Error bars represent 95% confidence interval. Individual measurements were obtained from the analysis of roots collected from a pool of 4 plants. Student's t test, ***$p < 0.001$.

E) Average change in primary root length of Col-0, *arsk1-1*, *arsk1-2*, *ARSK1-OE1* and *ARSK1-OE2* lines after 5 days of transfer to -P. DAT: days of transfer. Data shown from three biological repeats. Error bars represent 95% confidence interval. The letters represent statistically different means at $p < 0.05$ (one-way ANOVA with a Duncan post hoc test).

F) Representative images of wild-type Col-0, *arsk1-1*, and lines overexpressing genomic *ARSK1* (*ARSK1-OE1* and *ARSK1-OE2*) grown for 7 days in +P and -P are shown. Scale bars: 5 mm.

See also Figure S1, Table S1 and S2.

Figure 2. ARSK1 phosphorylates RAPTOR1B component of TORC1.

A) Yeast two-hybrid (Y2H) assays demonstrate ARSK1 interacts with RAPTOR1B. Yeast strains were plated on nonselective (NS) or on selective (S) medium. Each row shows ten-fold serial dilutions of the indicated strain.

B) ARSK1 phosphorylates RAPTOR1B in vitro. RAPTOR1B was TAP-purified from Arabidopsis PSB-d cell culture through its N- or C-terminal GS^{rhino} tag, and incubated with or without recombinant ARSK1 in the presence of ATP-P32. After 1h incubation, proteins were separated by SDS-PAGE and radioactivity was detected by autoradiography on a photographic film. The negative control with only ARSK1 indicates that ARSK1 is an active kinase that autophosphorylates (first lane). In the presence of ARSK1, the RAPTOR1B phosphosignal is higher compared to the negative controls without ARSK1. As additional negative control, ARSK1 was incubated with a TAP eluate from a wild-type PSB-d culture.

C) MSMS spectrum of phosphorylated (ph) Raptor1B peptide LAAASYWKPQS(0.331)S(0.331)S(0.331)LLTSLPSIAK with m/z 834.44. This peptide was

identified in all three replicate ARSK1 kinase assays with the Raptor1B-GSrhino TAP sample as substrate, while being absent from all three corresponding negative controls where ARSK1 was omitted. The y15 peak corresponds to the mass of the phosphorylated y-ion peptide, while the y15* peak reflects the mass of that ion with neutral loss -98 (H3PO4). The exact localization of the phosphorylation could not be derived from the spectrum, as reflected by a localization probability of 0.331 for each of the Serine residues at position 11, 12 and 13.
See also Figure S2, Table S2, S3 and S4.

Figure 3. Phosphorylation of RAPTOR1B S740 prevents growth inhibition in P deprived roots.

A) Average change in primary root length of Col-0, *arsk1-1*, *raptor1b*, and *raptor1b* plants expressing either a phosphomimicking (RAPTOR1B $S^{740}D$) or phosphodeficient (RAPTOR1B $S^{740}A$) RAPTOR1B. Plants were grown on complete medium for 5 days and then transferred to -P for 6 days. Primary root length were measured from 1 to 5 days after transfer (DAT). Data shown from three biological repeats, each experiment with 10 plants. Error bars represent 95% confidence interval.

B) Representative images of wild-type Col-0 and *raptor1b* plants expressing either a phosphomimicking (RAPTOR1B $S^{740}D$) or phosphodeficient (RAPTOR1B $S^{740}A$) RAPTOR1B. Scale bars: 5 mm.

C) Average change in primary root length of Col-0, *arsk1-1, raptor1b* lines expressing RAPTOR1B with a mutated Serine (S) at position 740 in arsk1raptor1b background replaced by alanine (A, RAPTOR1B S740A) or aspartic acid (D, RAPTOR1B S740D) after 5 days of transfer to -P. DAT: days of transfer. Data shown from three biological repeats, each experiment with 10 plants. Error bars represent 95% confidence interval. The letters represent statistically different means at $p < 0.05$ (one-way ANOVA with a Duncan post hoc test).

D) Average change in primary root length of Col-0, raptor1b, and raptor1b lines expressing phosphomimicking (aspartate (D)) or phosphodeficient (alanine (A)) RAPTOR1B forms for Serine (S) at position 739, 740, 741, 757 or threonine (T) for position 759. Plants were grown on complete medium for 5 days and then transferred to -P for 5 days. Primary root length were measured from day 1 to day 5 after transfer. DAT, day after transfer. Data shown from three biological repeats, each experiment with 10 plants. Error bars represent 95% confidence intervals. The letters represent statistically different means at $p < 0.05$ (one-way ANOVA with a Duncan post hoc test).

See also Figure S3 and Table S2.

Figure 4. ARSK1 influences RAPTOR1B stability and TOR activity in a P-dependent manner.

A) Immunological detection of RAPTOR1B protein in wild-type Col-0, *arsk1-1*, *ARSK1-OE1*, and *raptor1b* plants expressing either RAPTOR1B $S^{740}A$ or RAPTOR1B $S^{740}D$. Plants were grown on complete medium for 7 days and then transferred to -P for 9 hours. Seedling were used for this analysis. Coomassie is used as loading control in Western blot analysis. Arrowhead at about 150 kDa corresponds to the size of RAPTOR1B protein (148 kDa).

B-C) P availability influences TOR activity. The effect of combinatorial P and AZD-8055 (TOR inhibitor) treatments on primary root growth in Col-0 (**B**) and *arsk1-1* and *raptor1b* mutants lines after 5 days of transfer to each condition, (**C**) Data shown are from three experiments, each experiment with 10 plants. Error bars represent 95% confidence interval.

D) Immunological detection of S6K phosphorylation status in wild-type Col-0, *ARSK1-OE1*, *RAPTOR1B*$S^{740}D$ after 9 hours of transfer to +P or -P conditions. Apparent sizes of S6K-p, S6K: 52 kDa. Seedlings were used for this analysis. Coomassie is used as loading control in Western blot analysis.

E) Schematic model delineating a signaling pathway that integrates P availability cues to regulate root growth via TORC1. ARSK1 phosphorylates RAPTOR1B, and the phosphorylated RAPTOR1B promotes TOR activity to maintain root growth. P deficiency inhibits *ARSK1* expression, reduces RAPTOR1B accumulation, leading to reduced TOR activity. The decreased TOR activity triggers the inhibition of growth in P deprived roots.

See also Figure S3 and Table S2.

STAR★Methods

Resource availability

Lead contact

Further information and requests for resources and reagents should be directed to and will be fulfilled by a Lead Contact Hatem Rouached (rouached@msu.edu).

Materials availability

Transgenic plant seeds generated in this study are available from the Lead Contact on request.

Data and code availability

All data are available in the figures, tables, and data files associated with this manuscript. Transcriptome data were deposited in NCBI's Gene Expression Omnibus (GEO) under a project number GSE171449. This study did not result in any unique code. Any additional

information required to reanalyze the data reported in this paper is available from the lead contact upon request.

Experimental model and subject details

Arabidopsis (*Arabidopsis thaliana*) lines were in the Columbia-0 (Col-0) background as detailed in the Key resources table. Arabidopsis was grown in controlled growth conditions, as described in Method details.

Method details

Plant Growth Conditions

Seeds of *Arabidopsis thaliana* wild type (ecotype Columbia, Col-0, CS60000) and knock-out mutant lines in *RAPTOR1B* (AT3G08850) gene SALK_101990 and SALK_022096, were obtained from the Nottingham Arabidopsis Stock Centre (NASC). Homozygous mutant lines were confirmed by PCR using the primers listed in Supplemental Table S2. *ARSK1* (AT2G26290) overexpressed lines (*ARSK1-OE*1 and *ARSK1-OE2*) were generated by expressing *ARSK1* CDS in the *arsk1-1* mutant background (NASC, SALK_050925; *arsk1-2*, GABI_878C10). The *stop1* (SALK_114108), *almt1* (SALK_009629) were obtained from NASC. For 35Spro::GFP- ARSK1 and 35Spro::GFP- RAPTOR1B cloning, the full-length of ARSK1-attB-flanked and RAPTOR1Bs1-attB-flanked PCR product were obtained using specific primers. Using the gateway cloning vector set, the ARSK1 or RAPTORB1 were fused with GFP cloned in pMDC43[43] under the control of CaMV35S promoter (35Spro::GFP-ARSK1). The constructs were introduced into *Agrobacterium tumefaciens* strain GV3101. Point mutations T740A and T740D were introduced in RAPTOR1B sequence through a gene synthesis service by Genescript. Wild-type RAPTOR1B cDNA was also cloned through the same strategy. The attB-flanked DNA fragments were first sub-cloned into pDONR223 vector then into pMDC43 vector via the gateway system. The transgenic lines were generated with all the constructs in *raptor1b* and *arsk1-1*;*raptor1b* mutant backgrounds by Agrobacterium mediated transformation. Transgenic plants were selected by antibiotic (hygromycin) resistance, and only homozygous descendants of heterozygous T2 plants segregating 1:3 for antibiotic sensitivity: resistance were used for analysis. In total we had 4 homozygous lines showing similar phenotype. Arabidopsis plants were grown on control plates containing 1.249 mM KH_2PO_4; 0.25 mM $Ca(NO_3)_2$; 0.5 mM KNO_3; 1 mM $MgSO_4$; 100 µM $FeSO_4.7H_2O$; 30 µM H_3BO_3; 1 µM $ZnCl_2$; 10 µM $MnCl_2$; 1 µM $CuCl_2$; 0.1 µM $(NH_4)6Mo_7O_{24}$; and 50 µM KCl; 0.05% 2-(N-morpholino)ethanesulfonic acid (MES), 1% sucrose, and 0.8% washed agar. P-deficient media contained 12.49 µM KH_2PO_4 (+Fe-P). Fe-free media was obtained by omitting $FeSO_4.7H_2O$ from the growth media (+P-Fe). P- and Fe-deficient media contained 12.49 µM KH_2PO_4 (-P+Fe), and no $FeSO_4.7H_2O$ (-P-Fe). Seeds were stratified at 4°C for 3 days and

grown on square agar plates vertically in a growth chamber with 22°C, under long day regime (16H light/8H dark) at 100 µmol $m^{-2}s^{-1}$ fluorescent illumination. Plants were transformed by *Agrobacterium*-mediated transformation using the established floral dip method[44].

Agrobacterium-mediated transient expression was performed using *Agrobacterium* GV3101 strain as described[45]

Briefly, overnight-grown *Agrobacterium* culture was resuspended in induction medium (10 mM MES-KOH, pH 5.7, 10 mM $MgCl_2$, and 100 µM acetosyringone) to OD_{600}=0.2 and incubated for 2 hours at room temperature, before infiltration into *Nicotiana benthamiana* leaves. *Agrobacterium* strain carrying the 35Spro:p19 construct[46] was co-infiltrated to enhance the maximum levels of protein expression. Transiently expressed proteins were analyzed 2 days after infiltration with the Nikon A1Rsi CLSM microscope.

Genome Wide Expression Analysis

Total RNA was extracted from frozen and ground root tissues using TRIzolTM reagent (15596026, ThermoFisher Scientific) following the manufacturer's instructions. RNA integrity and concentration were determined using a 2100 Bioanalyzer Instrument (Agilent) and Agilent RNA 6000 Nano kit (5067-1511, Agilent). DNA contamination was removed by digestion with DNase I (AMPD1, SIGMA).

Genome-wide expression analysis in roots was based on 3 biological replicates obtained from independent experiments including four treatments (+P+Fe, +P-Fe, -P+Fe, -P-Fe) and 3 time points. Gene expression measurements were performed using Arabidopsis Affymetrix® Gene1.1 ST array strips designed to measure whole transcript accumulation of 28,501 genes (or transcripts clusters), based on 600,941 probes defined on TAIR10 genome annotation. Biotin labeled and fragmented cRNAs were obtained using a GeneChip® WT PLUS Reagent kit (902280, ThermoFisher Scientific) following manufacturer's instructions. Hybridization on array strips was performed for 16 hours at 48°C. Arrays were washed, stained, and scanned using a GeneAtlas HWS Kit (901667, ThermoFisher Scientific) on the GeneAtlas® Fluidics and Imaging Station.

Microarray raw data were processed with GCRMA available on the Expression Console Software developed by Affymetrix. Data analysis was performed in R version 4.2.1. Genes responding to the P and Fe treatment across time were identified using a three-way ANOVA that was modeled as follows: $Y= \mu + \alpha P + \beta Fe + \gamma Time + (\alpha\beta)P*Fe + (\alpha\gamma)P*Time + (\beta\gamma)Fe*Time + (\alpha\beta\gamma)P*Fe*Time + \varepsilon$, where Y is the normalized expression signal of a gene, µ is the global mean, the α, β and γ-coefficients correspond to the effects of P, Fe, and time (3,

6, 9 hours) and of the interaction between the factors, and ε represents the unexplained variance. All the genes for which all the coefficients are significant (p-value<0.05) were selected to explain variation of expression, except for the γTime coefficient only. Given the three-way ANOVA analysis, we retained differential expression events (p-value < 0.05) between genes in each experimental treatment (+P-Fe, -P+Fe, -P-Fe) per time point (3h, 6h, 9h) and the corresponding control treatments (+P/+Fe). This analysis identifies 242 of the 26,320 genes being differentially expressed in at least one experiment and time point.

Gene Regulatory Network Inference

Large-scale root specific gene expression compendium: We acquired a recently published, comprehensive study on gene expression for *A. thaliana*[47]. The collection had been subjected to consistent data processing and quality control. Given this dataset, we only retained conditions related to various stress and nutrient treatments in roots of *A. thaliana* ecotype Columbia-0. Subsequently, we transformed this condition-specific gene expression dataset into differential expression profiles computing the log fold change difference between individual treatments and corresponding control conditions. Our final differential expression dataset covered 82 % (21678 out of 26320 genes) of the *A. thaliana* genome and consisted of 66 differential expression profiles (**Table S1**).

Transcription factor binding information and family annotations: Most recent transcription factor family annotations were downloaded from iTAK[48]. Further, we acquired a comprehensive set of *A. thaliana* transcription factor binding motifs as positional weight matrices from Plantpan[49], covering in total 1011 transcription factors.

Gene regulatory network inference based on heterogeneous data integration: among the 242 genes that were differentially expressed in at least one of the iron and phosphate deficiency experiments, we identified 13 transcription factors (based on iTAK annotations). To derive a gene regulatory network architecture given these 13 transcription factors (TF) and 242 putative target genes (TG), we build an ensemble model of transcriptional regulation, integrating several heterogeneous features to derive a score per regulatory link between a TF and a TG.

Initially, putative causal co-differential expression of a TF and a TG was inferred based on whether the TF shows differential expression before or at the same time point as a TG in any of the three possible phosphate and iron experimental treatments (+P/-Fe, -P/+Fe, -P/-Fe). Here, each resulting putative regulatory relationship was annotated the experimental treatment.

Further, we elucidated putative binding of the TFs within the +1000bp to -200bp regions surrounding the transcription start site of TGs for all previously identified co-differentially expressed TF, TG pairs, using a custom R (V4.0.4) script based on the TFBSTools (V1.28.0) library. Positional weight matrices (PWM) were used as probabilistic binding motif representations to scan promoter sequences for the differentially expressed 242 genes, with promoter sequences acquired from TAIR10. To make PWM based promoter scanning more robust, we devised an ensemble strategy, i.e., we ran the algorithm several times with different model hyper-parameters and integrated the results of individual models into a continuous score ranging from 0 to 1. Hence, we set a minimum threshold > 0.5 corresponding to more than 50% of models supporting promoter binding for a specific TF, TG pair. If binding could not be observed we also removed the putative connection from the co-differential analysis, indicating that the previously identified co-differential expression between a TF and a TG is unlikely to have been caused by a direct regulatory interaction.

Given the limited number of TF binding motifs we covered only 6 (AT5G61430, AT1G77200, AT3G16280, AT4G17490, AT4G28790 and AT5G54230) of the 13 TFs. Hence, in order to evaluate the remaining 7 transcription factors' putative regulatory interactions on an additional dataset we established a supportive gene regulatory network. Therefore, we used a curated large-scale differential expression dataset of A. thaliana root stress treatments, covering 11 of the 13 TFs as well as 175 of the 242 TGs, and applied a robust random forest regression based approach[50] to estimate connections between TFs and TGs. Regression-based approaches to gene regulatory network inference assume that the expression profiles of the TFs that directly regulate a TG are the most informative, among all TFs, to predict the expression profile of the TG. Tree-based regression approaches, such as random forests, have proven successful as they can handle complex interaction and apply resampling strategies for repeated subsampling of the data, providing an inherent cross-validation. Random forest regression was performed with default parameters using all covered 11 regulators for all covered 175 putative target genes. Subsequently, we computed an empirical cumulative distribution function over all predictions assigning probabilities as continuous weights between 0 and 1 per regulatory link. Hence, we retained all previously identified co-differentially expressed TF, TG pairs, where binding analysis could not be performed due to missing motif information, as regulatory relationships if they had strong support (here defined as a probability of > 0.5) from the random forest based network inference.

Our final network contained 584 putative regulatory interactions between 12 transcription factors and 230 putative targets, each annotated to specific phosphate and iron experimental treatments or combinations thereof (**Table S1**).

Yeast Experiments

For the Y2H experiments, *ARSK1* and *RAPTOR1B* PCR products were obtained using high-fidelity Phusion DNA polymerase. The constructs were sequenced to ensure their integrity. Primers used for Y2H experiments are described in Supplemental Table S2. ARSK1 and RAPTOR1B were recombined into pDEST32, allowing fusion with the GAL4 DNA binding domain. Each pDEST22 and pDEST32 vector containing either ARSK1 or RAPTOR1B was transformed alone or in combination into yeast (AH109 strain; Clontech). Subsequent steps were conducted according to the manufacturer's instructions using the ADE2 HIS3 reporter genes (Clontech).

Real-time quantitative reverse-transcription PCR

Seeds of Arabidopsis wild type (Col-0) plants were germinated and grown for 7 days in control (+P) media and then transferred to -P. Root tissues were collected, and then used for total RNA extraction as described in[51,52]. Each experiment, per condition per genotype, was conducted with 12 plants and 4 plants were pooled for RNA extraction, resulting in 3 biological replicates. Two µg of the total RNA was used for reverse transcription (Invitrogen) to synthesize cDNA using oligo(dT) primer (Promega). Real-time quantitative reverse-transcription PCR (qRT-PCR) was performed as described in[51,53] using a LightCycler 480 Real-Time PCR System (Roche diagnostics). The *Ubiquitin 10* mRNA (*UBQ10*: AT4G05320) was used as a control to calculate the relative mRNA level of each gene.

In vitro Phosphorylation Assay

Production of recombinant ARSK1 kinase in *E. coli*. For gateway cloning of ARSK1, the ARSK1 CDS was synthesized together with the flanking attL1 and attL2 gateway sites into the pUC57-Km cloning vector (Genscript) and the resulting entry vector was cloned into pDest-HisMBP through standard LR gateway reaction. The resulting His-MBP expression vector was transformed into *E. coli* BL21 for production of recombinant ARSK1 as previously described[54].

In vitro Kinase Assays

For in vitro kinase assays, substrates were TAP-purified from PSB-D cell cultures expressing Raptor1B fused N- or C-terminally to the GSrhino TAP tag or LST8 fused C-terminally to the Gsrhino tag. As negative control, a mock TAP purification was performed on a wild-type PSB-D cell culture. TAP purifications were performed as described previously[55], with minor adjustments: phosphatase inhibitors (NaF, Na2VO4, β-glycerophosphate and p-NO2PhenylPO4) present in the TAP extraction buffer were added to all binding, wash and elution buffers, and protein complexes were not eluted from the Streptavidin beads. After

standard washing of Streptavidin beads, the beads were washed with kinase wash buffer (25 mM HEPES, pH 7.4, 20 mM KCl). Washed beads were dissolved in kinase assay buffer (25 mM HEPES, pH 7.4, 50 mM KCl, 10 mM MgCl2, 10 µM cold ATP). For P32 ATP kinase assays, kinase reactions were performed for 1 h at 30°C combining 20 µL TAP-purified substrates with 20 µL recombinant ARSK1 kinase, in the presence of 5 µCi γ-32P ATP. As negative control, 20 µL MBP elution buffer was added to the TAP-purified substrates instead of the ARSK1 kinase. Reactions were stopped by addition of SDS sample buffer and incubation for 10 min at 95°C. Proteins were separated by SDS-PAGE and stained with Coomassie brilliant blue R-250. Gels were dried and radioactivity was detected by autoradiography on a photographic film. For mass spectrometry-based identification of phosphopeptides, kinase assays were performed as described above, using 10 µM cold ATP instead of γ-32P ATP and reactions were incubated overnight at 30°C. Reactions were stopped by addition of NuPAGE sample buffer (ThermoFisher Scientific) and incubation at 70°C for 10 min. Proteins were separated for 7 min at 200V on a 4-12% NuPAGE gradient gel, stained with Coomassie G-250 and in-gel trypsin digested as described earlier[55].

LC−MS/MS analysis

Peptides were re-dissolved in 20 µl loading solvent A (0.1% TFA in water/I (98:2, v/v)) of which 5 µl was injected for LC-MS/MS analysis on an an Ultimate 3000 RSLC nano LC (Thermo Fisher Scientific, Bremen, Germany) in-line connected to a Q Exactive mass spectrometer (Thermo Fisher Scientific). The peptides were first loaded on a trapping column made in-house, 100 µm internal diameter (I.D.) × 20 mm, 5 µm beads C18 Reprosil-HD, Dr. Maisch, Ammerbuch-Entringen, Germany) and after flushing from the trapping column the peptides were separated on a 50 cm µPAC™ column with C18-endcapped functionality (Pharmafluidics, Belgium) kept at a constant temperature of 35°C. Peptides were eluted by a linear gradient from 98% solvent A' (0.1% formic acid in water) to 55% solvent B′ (0.1% formic acid in water/acetonitrile, 20/80 (v/v)) in 30 min at a flow rate of 300 nL/min, followed by a 5 min wash reaching 99% solvent B'. The mass spectrometer was operated in data-dependent, positive ionization mode, automatically switching between MS and MS/MS acquisition for the 5 most abundant peaks in each MS spectrum. The source voltage was 3.2 kV, and the capillary temperature was 275°C. One MS1 scan (m/z 400−2,000, AGC target 3 × 106 ions, maximum ion injection time 80 ms), acquired at a resolution of 70,000 (at 200 m/z), was followed by up to 5 tandem MS scans (resolution 17,500 at 200 m/z) of the most intense ions fulfilling predefined selection criteria (AGC target 5 × 104 ions, maximum ion injection time 80 ms, isolation window 2 Da, fixed first mass 140 m/z, spectrum data type: centroid, intensity threshold 1.3xE4, exclusion of unassigned, 1, 5-8, >8 positively charged precursors, peptide match preferred, exclude isotopes on, dynamic exclusion time 12 seconds). The HCD collision

energy was set to 25% Normalized Collision Energy and the polydimethylcyclosiloxane background ion at 445.120025 Da was used for internal calibration (lock mass). The raw files were processed with the MaxQuant software (version 1.6.10.43)[56], and searched with the built-in Andromeda search engine against the Araport11 plus database. This database consists of the Araport11 database with crap sequences (e.g. tags, keratins, trypsin etc. added). MaxQuant search parameters are listed in Supplemental Table S4.

Protein analysis

Arabidopsis seedling were grown for 10 day, then transferred on medium in presence of absence of P for 9 hours. For the immunoblotting, 100 mg plant tissue was ground in liquid nitrogen and suspended in 1.5 volume of extraction buffer (50 mM Tris–HCl pH 7.5, 150 mM NaCl, 10% glycerol, 5 mM dithiothreitol, 2 mM Na2MoO4, 2.5 mM NaF, 1.5 mM activated Na3VO4, 1 mM phenylmethanesulfonyl fluoride (PMSF), 1% IGEPAL, and cOmplete™ Protease Inhibitor Cocktail (Roche)). To obtain soluble protein, cell debris was removed by centrifugation 3 times. After denaturing with 6 × Laemmli buffer at 95°C for 5 minutes, 25 ug of protein were loaded into each well on the 10% SDS PAGE gel and transferred to the PVDF membrane (Bio-Rad, 1620174). The membrane were incubated in the blocking solution (5% skim milk) for 1h at room temperature (RT). For immunoblotting, RAPTOR1B primary antibody (PhytoAB, PHY2235S) was diluted to 1:750 and incubated overnight at 4°C. Anti-Rabbit IgG antibody (Sigma-Aldrich, A0545) diluted to 1:10000 was used as a secondary antibody for 2 hours at room temperature. TOR activity was assessed through the detection of S6K protein forms (phosphorylated and unphosphorylated forms), which were probed with Phospho-S6K antibody (Thr449, Abcam, ab207399) and S6K antibody (Cedarlane Labs, AS121855). Both antibodies were diluted to 1:2000 and incubated overnight at 4°C, The Goat anti-Rabbit IgG Antibody, HRP conjugate (Sigma-Aldrich, A0545, 1:4000 dilution) was used as secondary antibody. Immunoblotted bands were detected by Signalfire™ ECL Reagent (Cell Signaling Technology, 50-194-072 (6883S)) and visualized by Azure™ Biosystems Gel Doc.

Quantification and statistical analysis

Statistical analysis of quantitative data was performed using the GraphPad Prism 9 software program for macOS (Version 9.3.1 (350), December 7, 2021, USA, http://www.graphpad.com). When the test yielded a p-value <0.05, the difference for all the t-test analyses was considered statistically significant. Pearson correlation analysis was used to analyze the correlation.

SUPPLEMENTAL TABLE

Table S1. Predicted gene regulatory network with 584 putative regulatory interactions between 12 transcription factors and 230 putative targets, each annotated to specific phosphate and iron experimental treatments or combinations (Xls file), related Figure 1.

REFERENCES

1. Sánchez-Calderón, L., López-Bucio, J., Chacón-López, A., Cruz-Ramírez, A., Nieto-Jacobo, F., Dubrovsky, J.G., and Herrera-Estrella, L. (2005). Phosphate starvation induces a determinate developmental program in the roots of Arabidopsis thaliana. Plant Cell Physiol. *46*, 174–184.

2. Schmelzle, T., and Hall, M.N. (2000). TOR, a central controller of cell growth. Cell *103*, 253–262.

3. Henriques, R., Bögre, L., Horváth, B., and Magyar, Z. (2014). Balancing act: matching growth with environment by the TOR signalling pathway. J. Exp. Bot. *65*, 2691–2701.

4. Thomas, G., Sabatini, D.M., and Hall, M.N. (2012). TOR: Target of Rapamycin (Springer Science & Business Media).

5. Dobrenel, T., Caldana, C., Hanson, J., Robaglia, C., Vincentz, M., Veit, B., and Meyer, C. (2016). TOR Signaling and Nutrient Sensing. Annu. Rev. Plant Biol. *67*, 261–285.

6. Dobrenel, T., Mancera-Martínez, E., Forzani, C., Azzopardi, M., Davanture, M., Moreau, M., Schepetilnikov, M., Chicher, J., Langella, O., Zivy, M., et al. (2016). The Arabidopsis TOR Kinase Specifically Regulates the Expression of Nuclear Genes Coding for Plastidic Ribosomal Proteins and the Phosphorylation of the Cytosolic Ribosomal Protein S6. Front. Plant Sci. *7*, 1611.

7. Wu, Y., Shi, L., Li, L., Fu, L., Liu, Y., Xiong, Y., and Sheen, J. (2019). Integration of nutrient, energy, light, and hormone signalling via TOR in plants. J. Exp. Bot. *70*, 2227–2238.

8. Pfeiffer, A., Janocha, D., Dong, Y., Medzihradszky, A., Schöne, S., Daum, G., Suzaki, T., Forner, J., Langenecker, T., Rempel, E., et al. (2016). Integration of light and metabolic signals for stem cell activation at the shoot apical meristem. Elife *5*. 10.7554/eLife.17023.

9. Forzani, C., Duarte, G.T., Van Leene, J., Clément, G., Huguet, S., Paysant-Le-Roux, C., Mercier, R., De Jaeger, G., Leprince, A.-S., and Meyer, C. (2019). Mutations of the AtYAK1 Kinase Suppress TOR Deficiency in Arabidopsis. Cell Rep. *27*, 3696–3708.e5.

10. Dong, Y., Aref, R., Forieri, I., Schiel, D., Leemhuis, W., Meyer, C., Hell, R., and Wirtz, M. (2022). The plant TOR kinase tunes autophagy and meristem activity for nutrient stress-induced developmental plasticity. Plant Cell *34*, 3814–3829.

11. Song, L., Xu, G., Li, T., Zhou, H., Lin, Q., Chen, J., Wang, L., Wu, D., Li, X., Wang, L., et al. (2022). The RALF1-FERONIA complex interacts with and activates TOR signaling in response to low nutrients. Mol. Plant *15*, 1120–1136.

12. Belda-Palazón, B., Adamo, M., Valerio, C., Ferreira, L.J., Confraria, A., Reis-Barata, D., Rodrigues, A., Meyer, C., Rodriguez, P.L., and Baena-González, E. (2020). A dual function of SnRK2 kinases in the regulation of SnRK1 and plant growth. Nat Plants *6*, 1345–1353.

13. Nukarinen, E., Nägele, T., Pedrotti, L., Wurzinger, B., Mair, A., Landgraf, R., Börnke, F., Hanson, J., Teige, M., Baena-Gonzalez, E., et al. (2016). Quantitative phosphoproteomics reveals the role of the AMPK plant ortholog SnRK1 as a metabolic master regulator under energy deprivation. Sci. Rep. *6*, 31697.

14. Jamsheer K. M., J.K., Jindal, S., Sharma, M., Awasthi, P., Sreejath, S., Sharma, M., Mannully, C.T., and Laxmi, A. (2022). A negative feedback loop of TOR signaling balances growth and stress-response trade-offs in plants. Cell Reports *39*, 110631. 10.1016/j.celrep.2022.110631.

15. Cai, W., Li, X., Liu, Y., Wang, Y., Zhou, Y., Xu, T., and Xiong, Y. (2017). COP1 integrates light signals to ROP2 for cell cycle activation. Plant Signal. Behav. *12*, e1363946.

16. Poirier, Y., and Bucher, M. (2002). Phosphate transport and homeostasis in Arabidopsis. Arabidopsis Book *1*, e0024.

17. Nussaume, L., Kanno, S., Javot, H., Marin, E., Pochon, N., Ayadi, A., Nakanishi, T.M., and Thibaud, M.-C. (2011). Phosphate Import in Plants: Focus on the PHT1 Transporters. Front. Plant Sci. *2*, 83.

18. Abelson, P.H. (1999). A potential phosphate crisis. Science *283*, 2015.

19. Neset, T.-S., Cordell, D., Mohr, S., VanRiper, F., and White, S. (2016). Visualizing Alternative Phosphorus Scenarios for Future Food Security. Front Nutr *3*, 47.

20. Bouain, N., Cho, H., Sandhu, J., Tuiwong, P., Prom-u-thai, C., Zheng, L., Shahzad, Z., and Rouached, H. (2022). Plant growth stimulation by high CO2 depends on phosphorus homeostasis in chloroplasts. Curr. Biol. 32, 4493–4500.e4.

21. Ward, J.T., Lahner, B., Yakubova, E., Salt, D.E., and Raghothama, K.G. (2008). The effect of iron on the primary root elongation of Arabidopsis during phosphate deficiency. Plant Physiol. *147*, 1181–1191.

22. Balzergue, C., Dartevelle, T., Godon, C., Laugier, E., Meisrimler, C., Teulon, J.-M., Creff, A., Bissler, M., Brouchoud, C., Hagège, A., et al. (2017). Low phosphate activates STOP1-ALMT1 to rapidly inhibit root cell elongation. Nat. Commun. *8*, 15300.

23. Wang, X., Wang, Z., Zheng, Z., Dong, J., Song, L., Sui, L., Nussaume, L., Desnos, T., and Liu, D. (2019). Genetic Dissection of Fe-Dependent Signaling in Root Developmental Responses to Phosphate Deficiency. Plant Physiol. *179*, 300–316.

24. Czernic, P., Visser, B., Sun, W., Savouré, A., Deslandes, L., Marco, Y., Van Montagu, M., and Verbruggen, N. (1999). Characterization of an Arabidopsis thaliana receptor-like protein kinase gene activated by oxidative stress and pathogen attack. Plant J. *18*, 321–327.

25. Alassimone, J., Fujita, S., Doblas, V.G., van Dop, M., Barberon, M., Kalmbach, L., Vermeer, J.E.M., Rojas-Murcia, N., Santuari, L., Hardtke, C.S., et al. (2016). Polarly localized kinase SGN1 is required for Casparian strip integrity and positioning. Nat Plants *2*, 16113.

705 26. Rao, S., Zhou, Z., Miao, P., Bi, G., Hu, M., Wu, Y., Feng, F., Zhang, X., and Zhou, J.-M.
706 (2018). Roles of Receptor-Like Cytoplasmic Kinase VII Members in Pattern-Triggered
707 Immune Signaling. Plant Physiol. *177*, 1679–1690.

708 27. Du, C., Li, X., Chen, J., Chen, W., Li, B., Li, C., Wang, L., Li, J., Zhao, X., Lin, J., et al.
709 (2016). Receptor kinase complex transmits RALF peptide signal to inhibit root growth in
710 Arabidopsis. Proc. Natl. Acad. Sci. U. S. A. *113*, E8326–E8334.

711 28. Reymond, M., Svistoonoff, S., Loudet, O., Nussaume, L., and Desnos, T. (2006).
712 Identification of QTL controlling root growth response to phosphate starvation in
713 Arabidopsis thaliana. Plant Cell Environ. *29*, 115–125.

714 29. Müller J., Toev T., Heisters M., Teller J., Moore KL., Hause G., Dinesh DC.,
715 Bürstenbinder K., Abel, S. Iron-Dependent Callose Deposition Adjusts Root Meristem
716 Maintenance to Phosphate Availability (2015). Dev. Cell 33, 216–230.

717 30. Oughtred, R., Stark, C., Breitkreutz, B.-J., Rust, J., Boucher, L., Chang, C., Kolas, N.,
718 O'Donnell, L., Leung, G., McAdam, R., et al. (2019). The BioGRID interaction database:
719 2019 update. Nucleic Acids Research *47*, D529–D541. 10.1093/nar/gky1079.

720 31. Shahan, R., Hsu, C.-W., Nolan, T.M., Cole, B.J., Taylor, I.W., Greenstreet, L., Zhang,
721 S., Afanassiev, A., Vlot, A.H.C., Schiebinger, G., et al. (2022). A single-cell Arabidopsis
722 root atlas reveals developmental trajectories in wild-type and cell identity mutants.
723 Developmental Cell *57*, 543–560.e9. 10.1016/j.devcel.2022.01.008.

724 32. Aoki, Y., Okamura, Y., Tadaka, S., Kinoshita, K., and Obayashi, T. (2016). ATTED-II in
725 2016: A Plant Coexpression Database Towards Lineage-Specific Coexpression. Plant
726 Cell Physiol. *57*, e5.

727 33. Montané, M.-H., and Menand, B. (2013). ATP-competitive mTOR kinase inhibitors delay
728 plant growth by triggering early differentiation of meristematic cells but no
729 developmental patterning change. J. Exp. Bot. *64*, 4361–4374.

730 34. Barrada, A., Montané, M.-H., Robaglia, C., and Menand, B. (2015). Spatial Regulation
731 of Root Growth: Placing the Plant TOR Pathway in a Developmental Perspective. Int. J.
732 Mol. Sci. *16*, 19671–19697.

733 35. Anderson, G.H., Veit, B., and Hanson, M.R. (2005). The Arabidopsis AtRaptor genes
734 are essential for post-embryonic plant growth. BMC Biol. *3*, 12.

735 36. Chresta, C.M., Davies, B.R., Hickson, I., Harding, T., Cosulich, S., Critchlow, S.E.,
736 Vincent, J.P., Ellston, R., Jones, D., Sini, P., et al. (2010). AZD8055 is a potent,
737 selective, and orally bioavailable ATP-competitive mammalian target of rapamycin
738 kinase inhibitor with in vitro and in vivo antitumor activity. Cancer Res. *70*, 288–298.

739 37. Wullschleger, S., Loewith, R., and Hall, M.N. (2006). TOR signaling in growth and
740 metabolism. Cell *124*, 471–484.

741 38. Xiong, Y., and Sheen, J. (2014). The role of target of rapamycin signaling networks in
742 plant growth and metabolism. Plant Physiol. *164*, 499–512.

743 39. Bouain, N., Doumas, P., and Rouached, H. (2016). Recent Advances in Understanding
744 the Molecular Mechanisms Regulating the Root System Response to Phosphate
745 Deficiency in Arabidopsis. Curr. Genomics *17*, 308–304.

746 40. Dong, Y., Silbermann, M., Speiser, A., Forieri, I., Linster, E., Poschet, G., Allboje

Samami, A., Wanatabe, M., Sticht, C., Teleman, A.A., et al. (2017). Sulfur availability regulates plant growth via glucose-TOR signaling. Nat. Commun. *8*, 1174.

41. Jain, A., Poling, M.D., Karthikeyan, A.S., Blakeslee, J.J., Peer, W.A., Titapiwatanakun, B., Murphy, A.S., and Raghothama, K.G. (2007). Differential Effects of Sucrose and Auxin on Localized Phosphate Deficiency-Induced Modulation of Different Traits of Root System Architecture in Arabidopsis. Plant Physiology *144*, 232–247. 10.1104/pp.106.092130.

42. Burkart, G.M., and Brandizzi, F. (2021). A Tour of TOR Complex Signaling in Plants. Trends Biochem. Sci. *46*, 417–428.

43. Curtis, M.D., and Grossniklaus, U. (2003). A gateway cloning vector set for high-throughput functional analysis of genes in planta. Plant Physiol. *133*, 462–469.

44. Clough, S.J., and Bent, A.F. (1998). Floral dip: a simplified method for Agrobacterium-mediated transformation of Arabidopsis thaliana. Plant J. *16*, 735–743.

45. Cho, H.K., Ahn, C.S., Lee, H.-S., Kim, J.-K., and Pai, H.-S. (2013). Pescadillo plays an essential role in plant cell growth and survival by modulating ribosome biogenesis. Plant J. *76*, 393–405.

46. Marillonnet, S., Thoeringer, C., Kandzia, R., Klimyuk, V., and Gleba, Y. (2005). Systemic Agrobacterium tumefaciens-mediated transfection of viral replicons for efficient transient expression in plants. Nat. Biotechnol. *23*, 718–723.

47. He, F., Yoo, S., Wang, D., Kumari, S., Gerstein, M., Ware, D., and Maslov, S. (2016). Large-scale atlas of microarray data reveals the distinct expression landscape of different tissues in Arabidopsis. Plant J. *86*, 472–480.

48. Zheng, Y., Jiao, C., Sun, H., Rosli, H.G., Pombo, M.A., Zhang, P., Banf, M., Dai, X., Martin, G.B., Giovannoni, J.J., et al. (2016). iTAK: A Program for Genome-wide Prediction and Classification of Plant Transcription Factors, Transcriptional Regulators, and Protein Kinases. Mol. Plant *9*, 1667–1670.

49. O'Malley, R.C., Huang, S.-S.C., Song, L., Lewsey, M.G., Bartlett, A., Nery, J.R., Galli, M., Gallavotti, A., and Ecker, J.R. (2016). Cistrome and Epicistrome Features Shape the Regulatory DNA Landscape. Cell *165*, 1280–1292.

50. Petralia, F., Wang, P., Yang, J., and Tu, Z. (2015). Integrative random forest for gene regulatory network inference. Bioinformatics *31*, i197–i205.

51. Nam, H.-I., Shahzad, Z., Dorone, Y., Clowez, S., Zhao, K., Bouain, N., Lay-Pruitt, K.S., Cho, H., Rhee, S.Y., and Rouached, H. (2021). Interdependent iron and phosphorus availability controls photosynthesis through retrograde signaling. Nat. Commun. *12*, 7211.

52. Rouached, H., Wirtz, M., Alary, R., Hell, R., Arpat, A.B., Davidian, J.-C., Fourcroy, P., and Berthomieu, P. (2008). Differential regulation of the expression of two high-affinity sulfate transporters, SULTR1.1 and SULTR1.2, in Arabidopsis. Plant Physiol. *147*, 897–911.

53. Bouain, N., Cho, H., Sandhu, J., Tuiwong, P., Prom-U-Thai, C., Zheng, L., Shahzad, Z., and Rouached, H. (2022). Plant growth stimulation by high CO depends on phosphorus homeostasis in chloroplasts. Curr. Biol. 10.1016/j.cub.2022.08.032.

54. Van Leene, J., Han, C., Gadeyne, A., Eeckhout, D., Matthijs, C., Cannoot, B., De Winne, N., Persiau, G., De Slijke E, V., de Cotte B, V., et al. (2019). Capturing the phosphorylation and protein interaction landscape of the plant TOR kinase. Nature plants *5*. 10.1038/s41477-019-0378-z.

55. Van Leene, J., Eeckhout, D., Cannoot, B., De Winne, N., Persiau, G., De Slijke E, V., Vercruysse, L., Dedecker, M., Verkest, A., Vandepoele, K., et al. (2015). An improved toolbox to unravel the plant cellular machinery by tandem affinity purification of Arabidopsis protein complexes. Nat. Protoc. *10*. 10.1038/nprot.2014.199.

56. Cox, J., and Mann, M. (2008). MaxQuant enables high peptide identification rates, individualized p.p.b.-range mass accuracies and proteome-wide protein quantification. Nat. Biotechnol. *26*, 1367–1372.

Key Ressource Table

REAGENT or RESOURCE	SOURCE	IDENTIFIER
Bacterial and virus strains		
Agrobacterium tumefaciens (GV3101)	N/A	N/A
E. Coli (TOP10)	Thermo Fisher	Cat#C404010
E. Coli (BL21)	Invitrogen	Cat#C600003
Yeast (AH109)	Clontech	N/A
Chemicals, peptides, and recombinant proteins		
Iron(III) sulfate hydrate	Millipore Sigma	Cat#307718
2,2'-bipyridine	Millipore Sigma	Cat#D216305
Thioglycolic acid	Millipore Sigma	Cat#T3758
deoxynucleotide triphosphate (dNTP)	Promega	Cat#U1205
Superscript III Reverse transcriptase	Invitrogen	Cat#18080093
SYBR Green Master Mix	Roche	Cat#04707516001
Critical commercial assays		
RNeasy Plant Mini Kit	QIAGEN	Cat#74904
RAPTOR1B	PhytoAB,	Cat#PHY2235S
Phospho-S6K antibody (Thr449)	Abcam	Cat#ab207399
S6K 1/2	Cedarlane Labs	Cat#AS12
α-Tubulin	Sigma-Aldrich	Cat#T6199
Experimental models: Organisms/strains		
Arabidopsis thaliana, Col-0 ecotype (WT)	N/A	N/A
Arabidopsis *arsk1-1*;*raptor1b*	This study	N/A
Arabidopsis 35Spro::GFP- ARSK1	This study	N/A

Arabidopsis 35Spro::GFP- RAPTOR1B	This study	N/A
Arabidopsis proARSK1::GUS	This study	N/A
Arabidopsis proRAPTOR1B::GUS	This study	N/A
Arabidopsis RAPTOR1BS^{740}A in *raptor1b*	This study	N/A
Arabidopsis RAPTOR1BS^{740}A in *arsk1;raptor1b*	This study	N/A
Arabidopsis RAPTOR1BS^{740}D in *raptor1b*	This study	N/A
Arabidopsis RAPTOR1BS^{740}D in *arsk1;raptor1b*	This study	N/A
Arabidopsis RAPTOR1BS^{739}A in *raptor1b*	This study	N/A
Arabidopsis RAPTOR1BS^{739}D in *raptor1b*	This study	N/A
Arabidopsis RAPTOR1BS^{741}A in *raptor1b*	This study	N/A
Arabidopsis RAPTOR1BS^{741}D in *raptor1b*	This study	N/A
Arabidopsis RAPTOR1BS^{757}A in *raptor1b*	This study	N/A
Arabidopsis RAPTOR1BS^{757}D in *raptor1b*	This study	N/A
Arabidopsis RAPTOR1BS^{759}A in *raptor1b*	This study	N/A
Arabidopsis RAPTOR1BS^{759}D in *raptor1b*	This study	N/A
Arabidopsis, AT2G26290	ABRC	SALK_050925
Arabidopsis, AT2G26290	ABRC	GABI_878C10
Arabidopsis, AT3G08850	ABRC	SALK_101990
Arabidopsis, AT3G08850	ABRC	SALK_022096
Arabidopsis, AT1G34370	ABRC	SALK_114108
Arabidopsis, AT1G08430	ABRC	SALK_009629
Nicotiana Benthamiana	N/A	N/A
Oligonucleotides		
Table S2 in the supplemental information	This study	N/A

Recombinant DNA		
35Spro::GFP- ARSK1	This study	N/A
35Spro::GFP- RAPTOR1B	This study	N/A
proARSK1::GUS	This study	N/A
proRAPTOR1B::GUS	This study	N/A
RAPTOR1BS^{740}A	This study	N/A
RAPTOR1BS^{740}A	This study	N/A
RAPTOR1BS^{739}A	This study	N/A
RAPTOR1BS^{739}D	This study	N/A
RAPTOR1BS^{741}A	This study	N/A
RAPTOR1BS^{741}D	This study	N/A
RAPTOR1BS^{757}A	This study	N/A
RAPTOR1BS^{757}D	This study	N/A
RAPTOR1BS^{759}A	This study	N/A
RAPTOR1BS^{759}D	This study	N/A
His-MBP-ARSK1	This study	N/A
Other		
Prism	Prism9	https://www.graphpad.com/

Figure 1

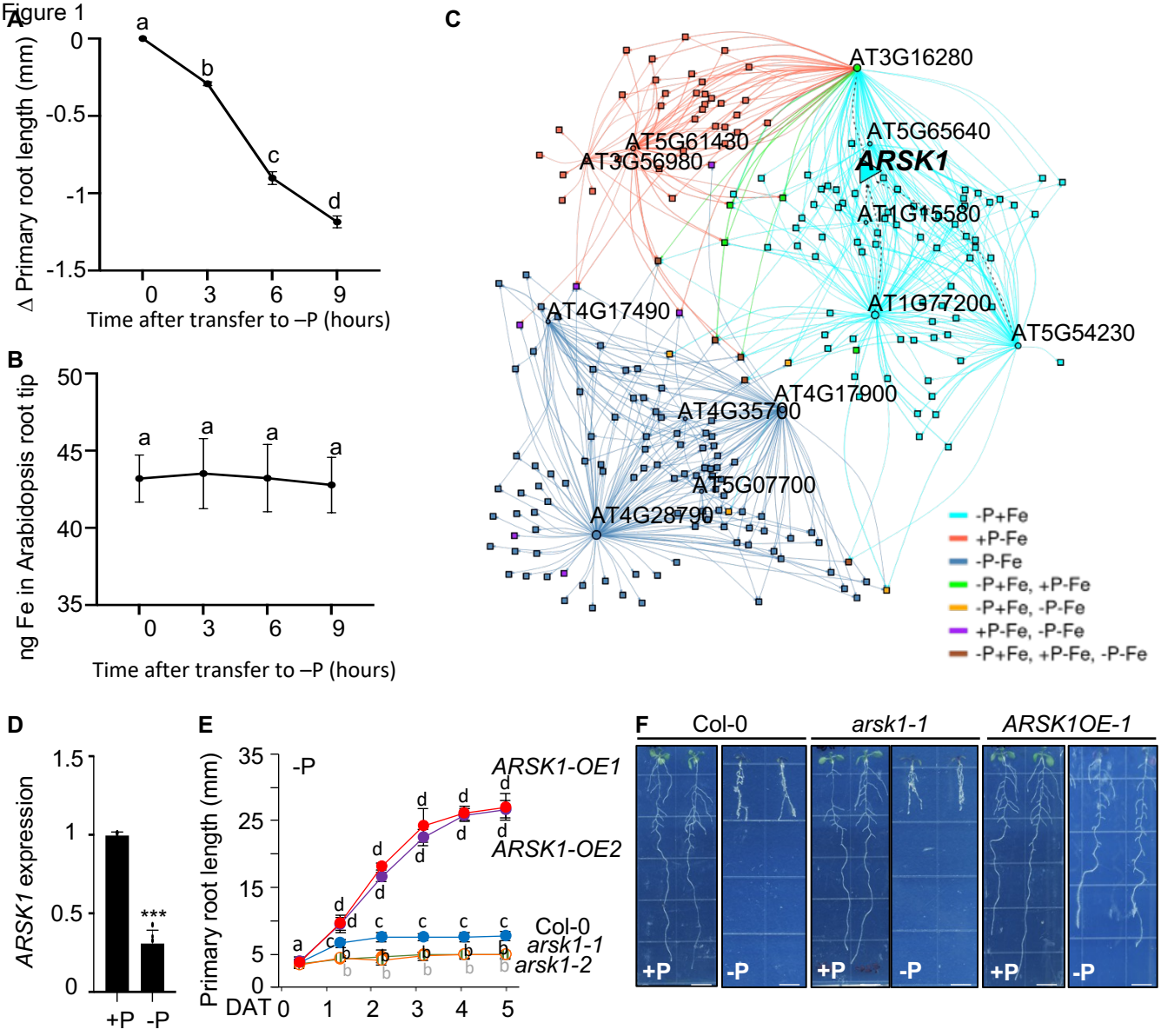
A
Δ Primary root length (mm)
0
-0.5
-1
-1.5
a
b
c
d
0
3
6
9
Time after transfer to –P (hours)
B
ng Fe in Arabidopsis root tip
50
45
40
35
a
a
a
a
0
3
6
9
Time after transfer to –P (hours)
C
AT3G16280
AT5G65640
AT5G61430
AT3G56980
ARSK1
AT1G15580
AT4G17490
AT1G77200
AT5G54230
AT4G17900
AT4G35700
AT5G07700
AT4G28790
-P+Fe
+P-Fe
-P-Fe
-P+Fe, +P-Fe
-P+Fe, -P-Fe
+P-Fe, -P-Fe
-P+Fe, +P-Fe, -P-Fe
D
ARSK1 expression
1.5
1
0.5
0
***
+P
-P
E
Primary root length (mm)
35
25
15
5
0
-P
ARSK1-OE1
ARSK1-OE2
Col-0
arsk1-1
arsk1-2
DAT 0
1
2
3
4
5
F
Col-0
arsk1-1
ARSK1OE-1
+P
-P
+P
-P
+P
-P

Figure 2

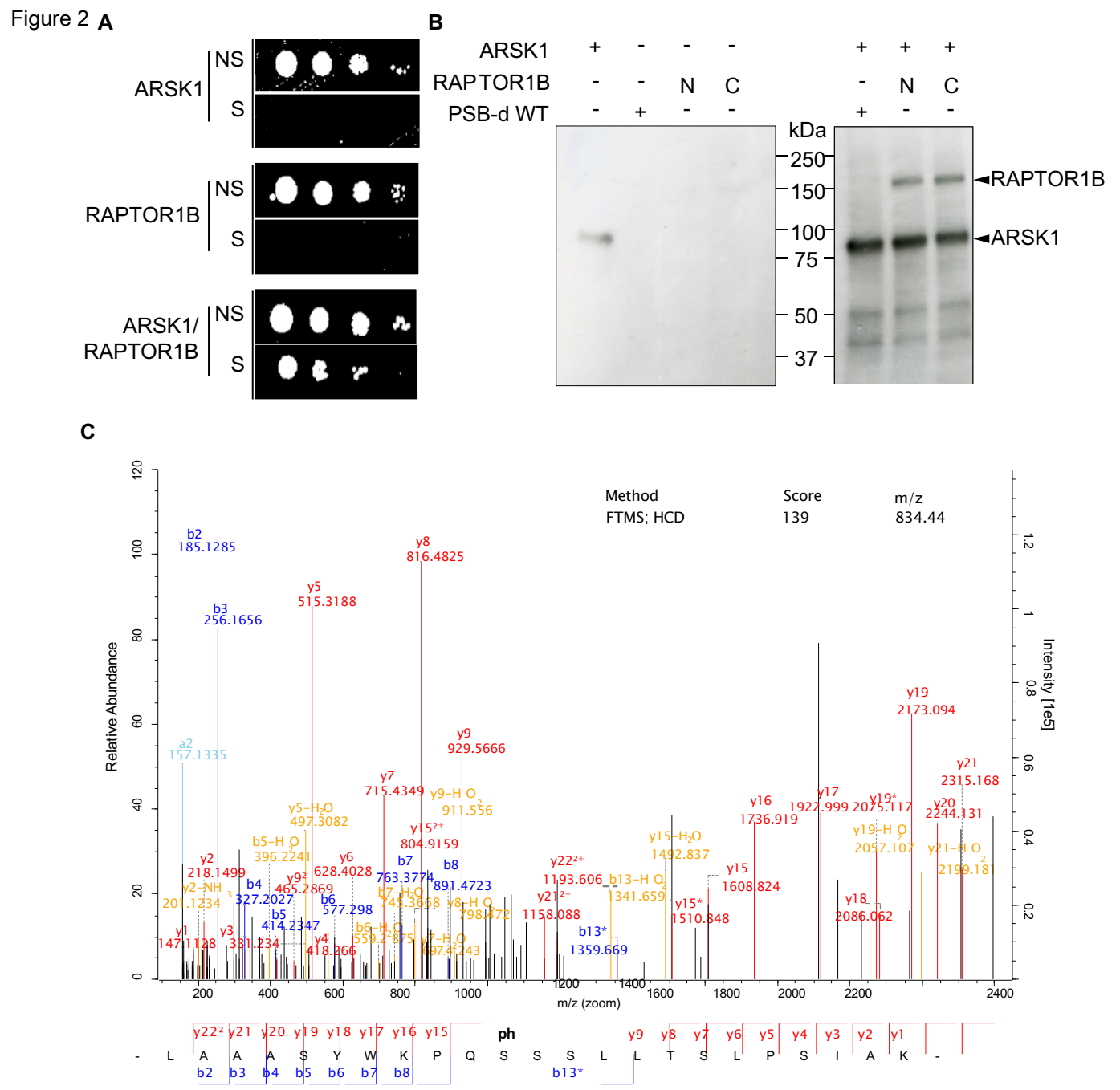
A
ARSK1
NS
S
RAPTOR1B
NS
S
ARSK1/
RAPTOR1B
NS
S
B
ARSK1 + - - - + + +
RAPTOR1B - - N C - N C
PSB-d WT - + - - + - -
kDa
250
150
100
75
50
37
RAPTOR1B
ARSK1
C
Method
FTMS; HCD
Score
139
m/z
834.44
Relative Abundance
Intensity [1e5]
m/z (zoom)
b2 185.1285
y8 816.4825
y5 515.3188
b3 256.1656
y9 929.5666
y7 715.4349
y19 2173.094
y21 2315.168
y16 1736.919
y17 1922.999
y20 2244.131
y15 1608.824
y18 2086.062
y22²⁺ 1193.606
y21²⁺ 1158.088
b13* 1359.669
y15* 1510.848
ph
- L A A A S Y W K P Q S S S L L T S L P S I A K -
b2 b3 b4 b5 b6 b7 b8 b13*
y22² y21 y20 y19 y18 y17 y16 y15 y9 y8 y7 y6 y5 y4 y3 y2 y1

Figure 3

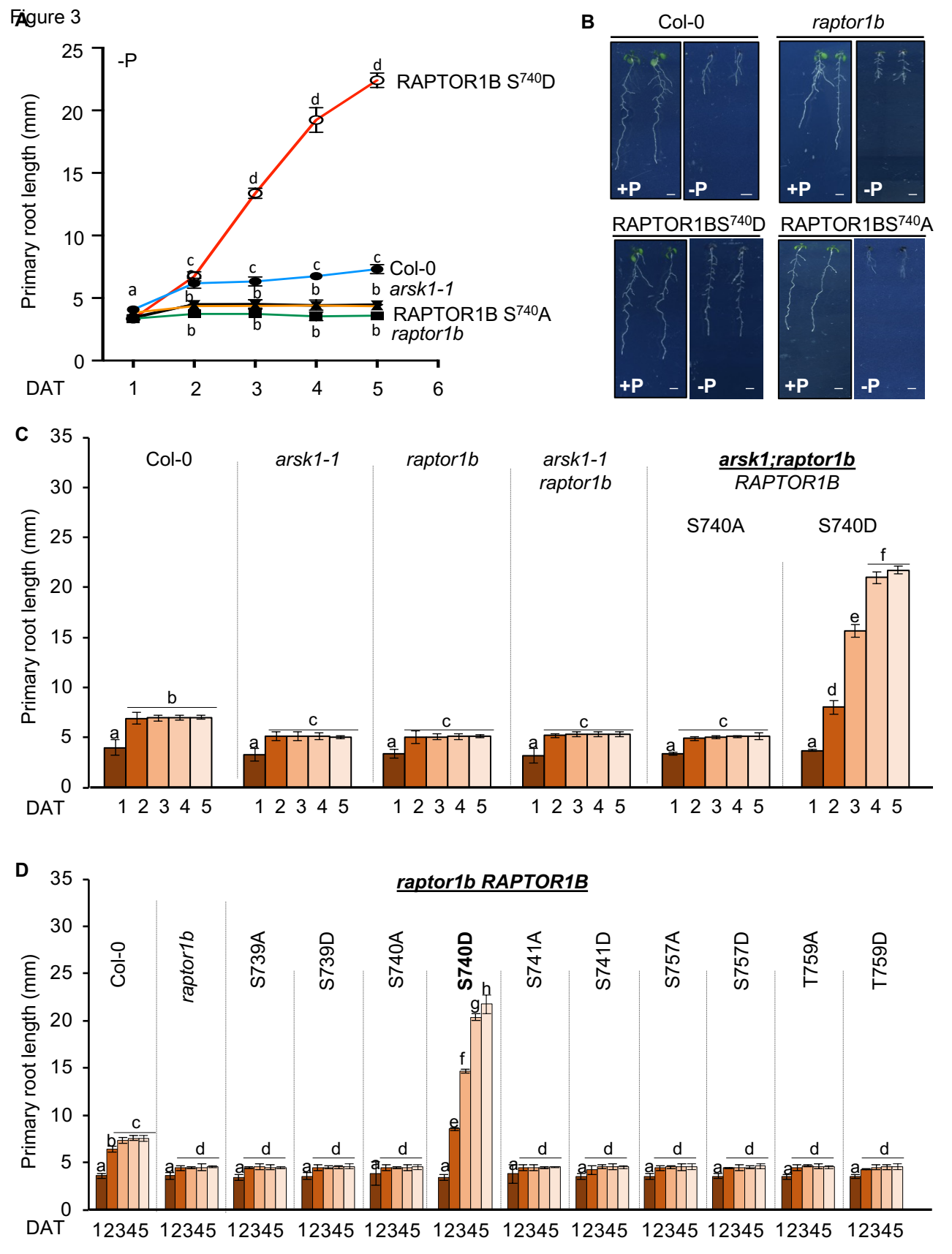
A
-P
Primary root length (mm)
DAT
RAPTOR1B S740D
Col-0
arsk1-1
RAPTOR1B S740A
raptor1b
B
Col-0
raptor1b
+P
-P
RAPTOR1BS740D
RAPTOR1BS740A
C
Col-0
arsk1-1
raptor1b
arsk1-1 raptor1b
arsk1;raptor1b RAPTOR1B
S740A
S740D
D
raptor1b RAPTOR1B
Col-0
raptor1b
S739A
S739D
S740A
S740D
S741A
S741D
S757A
S757D
T759A
T759D

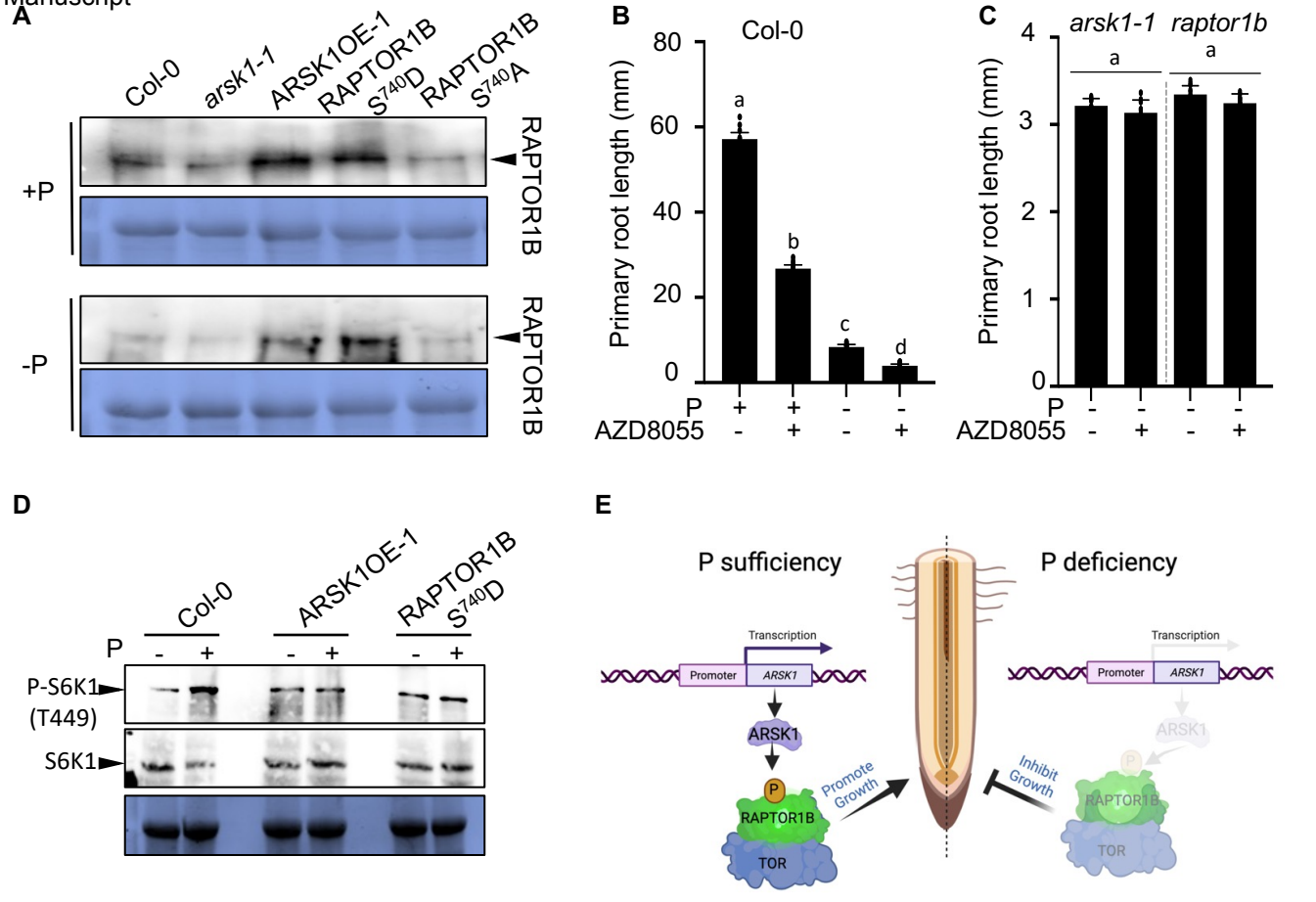
A
Col-0
arsk1-1
ARSK1OE-1
RAPTOR1B
S740D
RAPTOR1B
S740A
+P
-P
RAPTOR1B
RAPTOR1B
B
Col-0
Primary root length (mm)
80
60
40
20
0
a
b
c
d
P + + - -
AZD8055 - + - +
C
arsk1-1
raptor1b
a
a
Primary root length (mm)
4
3
2
1
0
P - - - -
AZD8055 - + - +
D
Col-0
ARSK1OE-1
RAPTOR1B
S740D
P - + - + - +
P-S6K1
(T449)
S6K1
E
P sufficiency
P deficiency
Transcription
Promoter
ARSK1
ARSK1
P
RAPTOR1B
TOR
Promote
Growth
Inhibit
Growth
Transcription
Promoter
ARSK1
ARSK1
P
RAPTOR1B
TOR

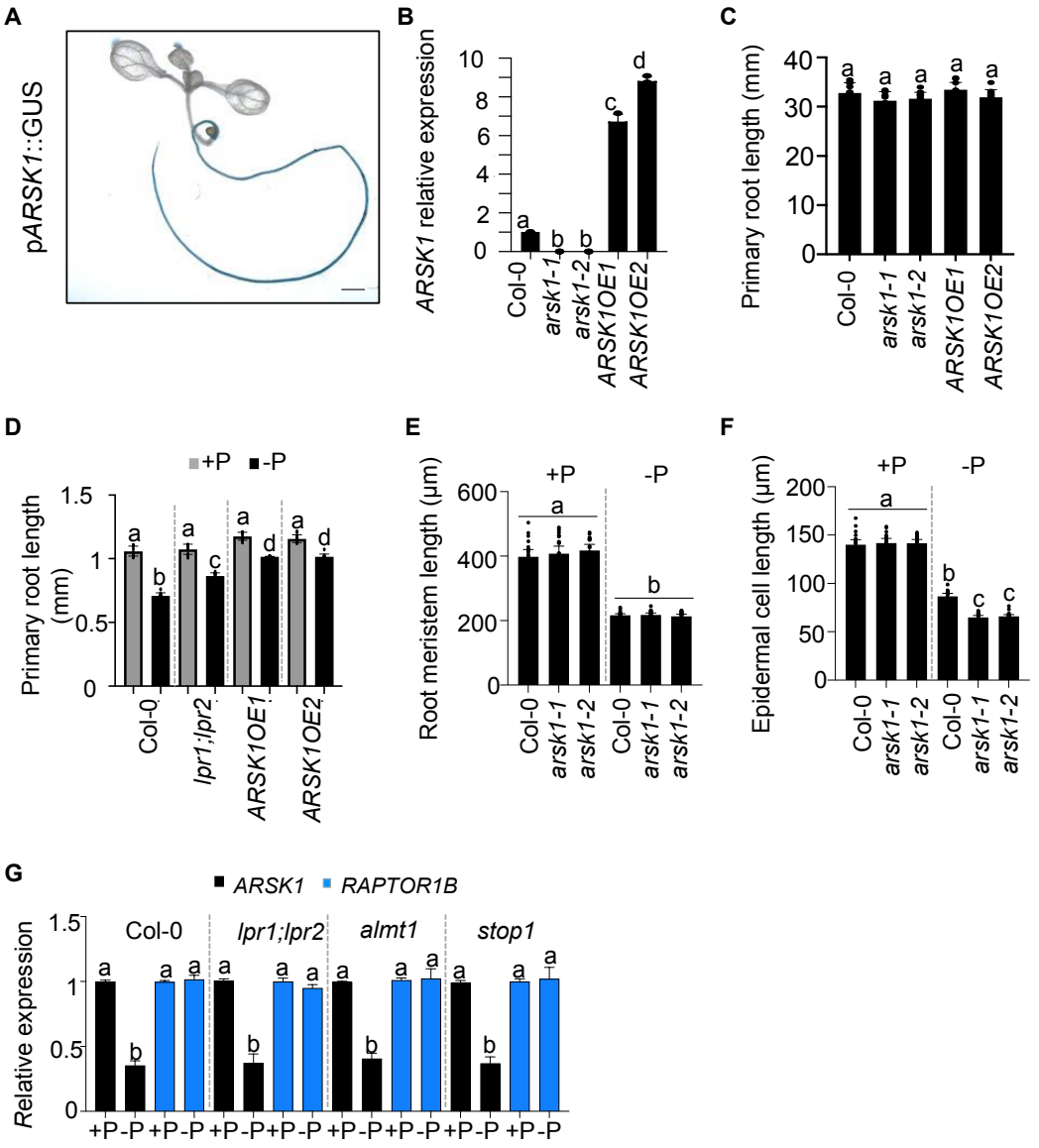

Figure S1 Plants overexpressing *ARSK1* display longer roots compared to the *lpr1*;*lpr2* mutants, related to Figure 1.

A) Two-week-old seedling expressing GUS reporter gene under the control of ARSK1 promoter. Scale bar, 1 mm.

B) Relative mRNA abundance of the *ARSK1* gene in roots of Col-0, *arsk1-1, arsk1-2*, *ARSK1-OE1*, and *ARSK1-OE2*. Data (means ± 95% confidence interval) from 3 independent plant cultures, each with a pool of 6 plants per genotype. Letters denote significant differences at $p < 0.05$, one-way ANOVA with a Duncan post hoc test.

C) Average change in primary root length of Col-0, *arsk1-1, arsk1-2*, *ARSK1-OE1* and *ARSK1-OE2* lines after 5 days of transfer (DAT) to +P. Data shown are from three biological repeats. Error bars represent 95% confidence interval. The letters correspond to statistically different means at $p < 0.05$ (one-way ANOVA with a Duncan post hoc test).

D) Average change in primary root length of Col-0, *ARSK1-OE1*, *ARSK1-OE2*, and *lpr1;lpr2* mutants after 9 hours of transfer to -P. Data shown are from three biological repeats, each

experiment with 10 plants. Error bars represent 95% confidence interval. The letters correspond to statistically different means at $p < 0.05$ (one-way ANOVA with a Duncan post hoc test).
E) Primary root meristem length in Col-0, *arsk1-1* and *arsk1-2* lines after 2 days of transfer to -P (n=21 meristems per condition). The letters represent statistically different means at $p < 0.05$ (one-way ANOVA with a Duncan post hoc test).
F) The length of root epidermal cells within the elongation zone. Col-0, *arsk1-1* and *arsk1-2* plants were grown for 3 days in +P then transferred to +P or –P medium for 2 additional days (n=21 meristems per condition). The letters represent statistically different means at $p < 0.05$ (one-way ANOVA with a Duncan post hoc test).
G) Relative mRNA expression of the *ARSK1* and *RAPTOR1B* genes in the roots of Col-0, *lpr1;lpr2, almt1*, and *stop1* mutants. mRNAs were extracted from roots of plants grown on the normal medium for 5 days and transferred to the -P or +P medium for 9 hours. The letters represent statistically different means at $p < 0.05$ (one-way ANOVA with a Duncan post hoc test).

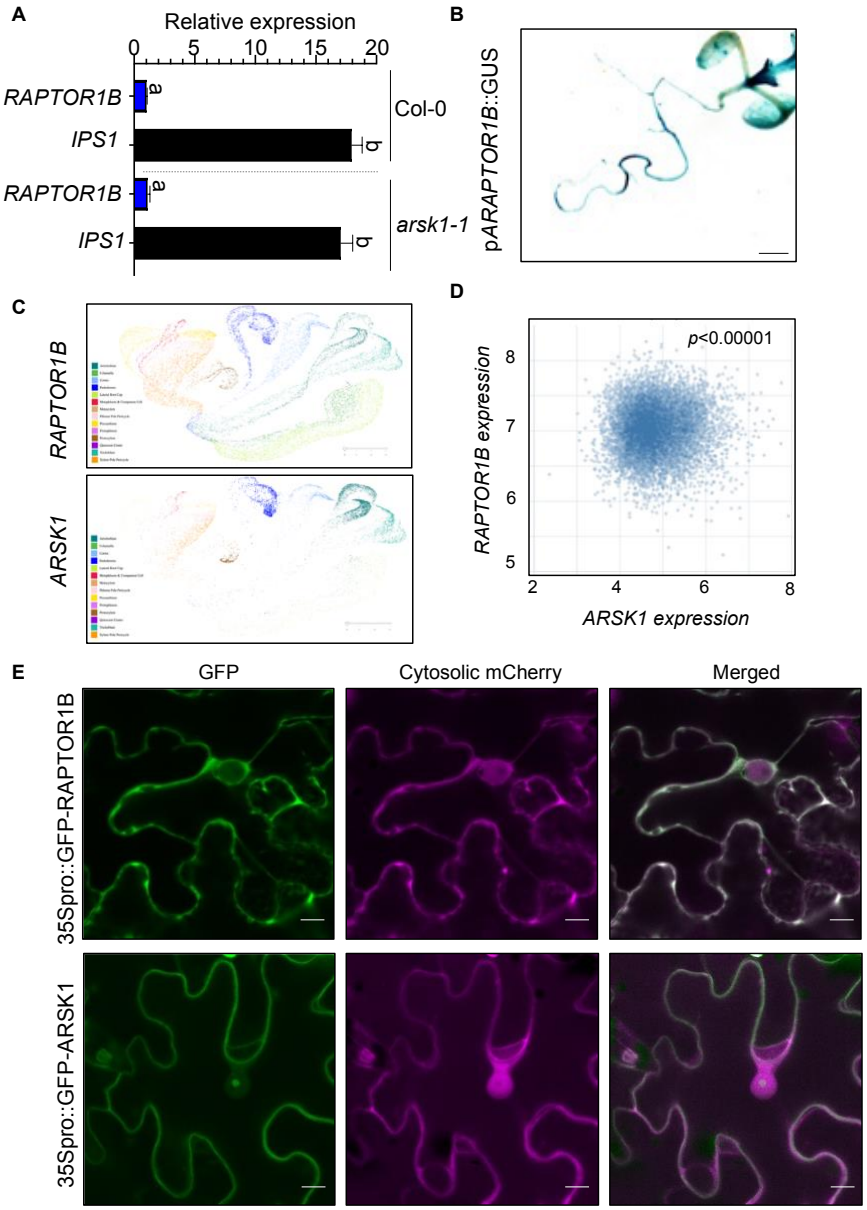

Figure S2 ARSK1 and RAPTOR1B expression overlaps, related to Figure 2.
A) Relative mRNA abundance of *RAPTOR1B* and *INDUCED BY PHOSPHATE STARVATION 1 (IPS1*) in the Col-0 and *arsk1-1* plants grown for 7 days and transferred to -P for 9 hours. The letters represent statistically different means at p < 0.05 (one-way ANOVA with a Duncan post hoc test)
B) Two-week-old seedling expressing GUS reporter gene under the control of *RAPTOR1B* promoter. Scale bar, 1 mm.
C) Expression of *RAPTOR1B* and *ARSK1* in major Arabidopsis root cell types using phytozome.
D) Co-expression analysis of *ARSK1* and *RAPTOR1B* using Arabidopsis ATTEDII database (https://atted.jp/). *p*-value is presented.
E) Subcellular localization ARSK1 and RAPTOR1B in tobacco leaves. 35Spro::GFP-ARSK1 and 35Spro::GFP-RAPTOR1B were transiently expressed in *N. benthamiana* leaves with the cytosolic mCherry marker via agroinfiltration. The infiltrated leaves were examined by confocal laser scanning microscopy. Scale bars, 10μm.

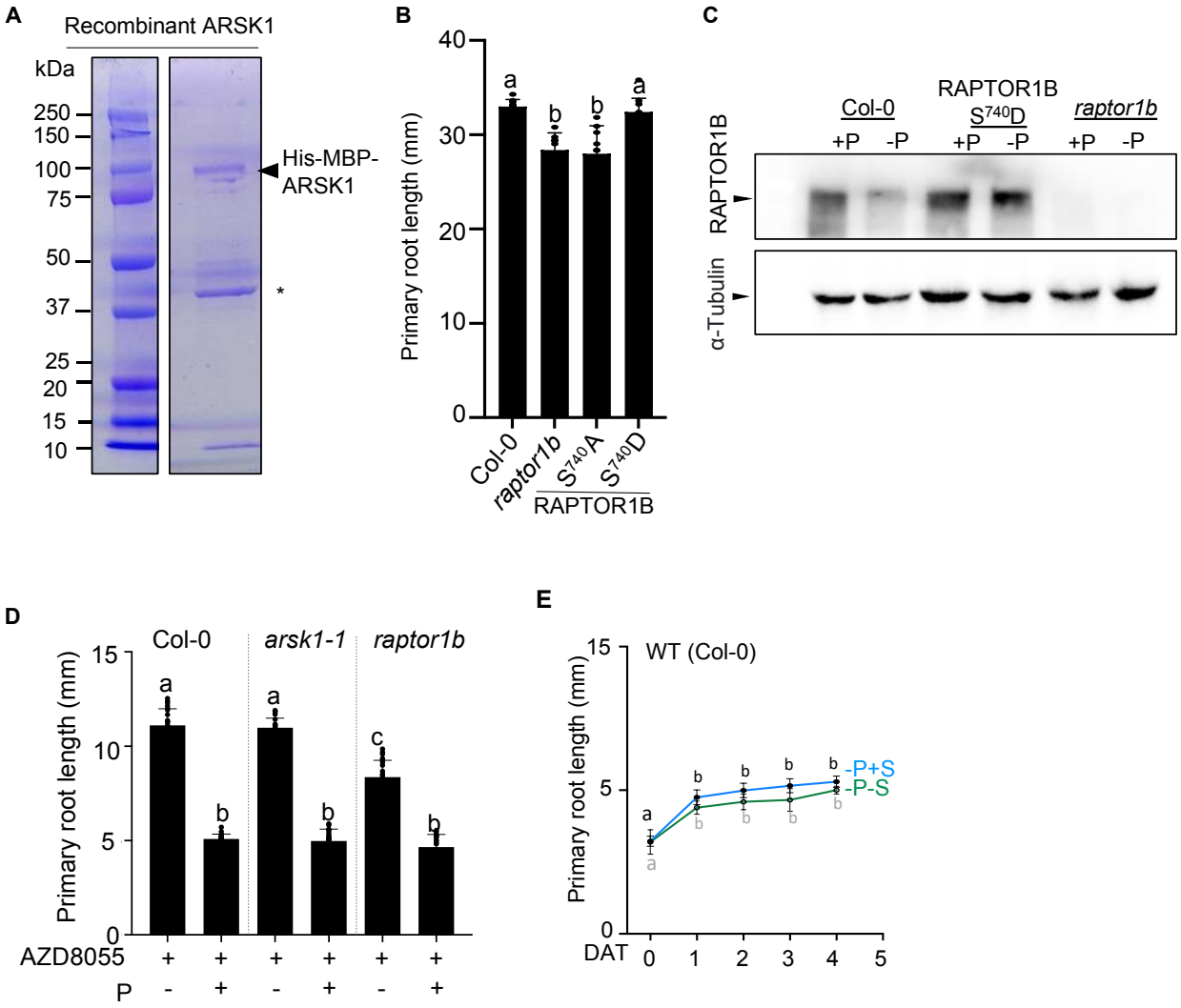

Figure S3 P availability influences TOR activity, related to Figures 3 and 4.

A) Purity of recombinant ARSK1**.** Coomassie R staining of the His-MBP-ARSK1 recombinant protein purified from *E. coli* on an amylose resin. The asterisk represents the His-MBP tag (42.8kDa) as such resulting from degradation during the purification.

B) Average primary root length of Col-0, *raptor1b*, RAPTOR1B S740D and RAPTOR1B S740A plants grown in +P for 5 days and transferred on the same condition (+P) for 5 additional days. Data shown are from three biological repeats, each experiment with 10 plants. Error bars represent 95% confidence interval.

C) The expression of RAPTOR1B protein in the roots of wild type Col-0, *raptor1b*, and *raptor1b* expressing RAPTOR1B S740D. The protein samples were prepared after transferring 7 days old plants under the -P or +P conditions for 9 hours. Arrowhead at about 150 kDa corresponds to the size of RAPTOR1B protein (148 kDa) and about 50 kDa corresponds to the size of α-Tublulin.

D) The effect of combinatorial P and AZD-8055 (TOR inhibitor) treatments on primary root growth in Col-0 and *arsk1-1* and *raptor1b* mutants lines. All plants were grown for 3 days in +P then transferred to indicated conditions for 5 additional days. Data shown are from three experiments. Error bars represent 95% confidence interval. The letters represent statistically different means at $p < 0.05$ (one-way ANOVA with a Duncan post hoc test).

E) Average change in primary root length of Col-0 lines after 5 days of transfer to -P with 1% sucrose (-P+S) or without sucrose (-P-S). Data shown are from three biological repeats. Error bars represent 95% confidence interval. The letters represent statistically different means at $p < 0.05$ (one-way ANOVA with a Duncan post hoc test).

Name/ Genes	Purpose	Sequence
arsk1-1 (SALK_050925)	T-DNA insertion mutant	LP: CTTCATCCTTATTCCCCAAGC RP: CCATGTCGGTTATGGATGATC
arsk1-2 (GABI_878C10)	T-DNA insertion mutant	LP: TGAAGATCAAGAGCCTTTACAGCA RP: AAACAAAGTCAACGGACATCCAAT
raptor1B (SALK_101990)	T-DNA insertion mutant	LP: AGCAGTGACGGATACAATTGC RP: GTTGTTTGCAGAAGCTTCAGC
raptor1B (SALK_022096)	T-DNA insertion mutant	LP: CAATATGAAGCTGCGGCTAAC RP: CATCGGATCAAGTTGCTTACC
stop1 (SALK_114108)	T-DNA insertion mutant	LP: CCACCAAACGTGAAGAGAGAG RP: ATGAAGCACAGGACCATGATC
almt1 (SALK_009629)	T-DNA insertion mutant	LP: GAAATTATTTGGGGAAGCTGC RP: TCTTTACCCATGGGAAAAACC
ARSK1 (AT2G26290)	Overexpression line / Y2H	F: AAAAAGCAGGCTCCATGGCAGTGTTCA R: AGAAAGCTGGGTCTCAAATGCCATCGT
RAPTOR1B (AT3G08850)	Overexpression line / Y2H	F: AAAAAGCAGGCTCCATGGCATTAGGAG R: AGAAAGCTGGGTCTCATCTTGCTTGCGA
ARSK1 (AT2G26290)	Gene-GFP / transient expression	F: AAAAAGCAGGCTCCATGGCAGTGTTCA R: AGAAAGCTGGGTCTCAAATGCCATCGT
RAPTOR1B (AT3G08850)	Gene-GFP / transient expression	F: AAAAAGCAGGCTCCATGGCATTAGGAG R: AGAAAGCTGGGTCTCATCTTGCTTGCGA
ARSK1 (AT2G26290)	Promoter-GUS	F: AAAAAGCAGGCTCCCGAACAATTTAAT R: AGAAAGCTGGGTCTTTCAACTTCTTCT
RAPTOR1B (AT3G08850)	Promoter-GUS	F: AAAAAGCAGGCTCCGCTAGGAGTTGAG R: AGAAAGCTGGGTCCCAAATCGGAGAA
ARSK1 (AT2G26290)	qPCR	F: GGTTGCTGTAAAGGCTCTTGAT R: TGTTTGTTACTTAGTTGTCCCAAAA
RAPTOR1B (AT3G08850)	qPCR	F: CAACGACATCTCACACTCC R: CAAACTCTCCTCAATCCACTC
IPS1 (AT3G09922)	qPCR	F: GCAGAAGGCTGATTCAGAC R: CTCACACAAAGAACACACAAC
Ubiquitin10 (AT4G05320)	qPCR	F: GTCCACCCTTCATCTTGTTC R: CTGCCATCTTCAAGTTGTTTTC

Table S2. The primers used in this study, related Figures 1-4, S1-S3.

Protein	Fasta headers	Amino acid	Positions within proteins	Phospho (STY) Probabilities	Phospho (STY) Score diffs
AT3G08850.1	RAPTOR1B | Regulatory-associated protein of TOR 1 | 201606	S	739	LAAASYWKPQS(0.331)S(0.331)S(0.331)LLT(0.007)S(0.001)LPSIAK	LAAAS(-58)Y(-71)WKPQS(0)S(0)S(0)LLT(-17)S(-26)LPS(-38)IAK
		S	740	LAAASYWKPQS(0.331)S(0.331)S(0.331)LLT(0.007)S(0.001)LPSIAK	LAAAS(-58)Y(-71)WKPQS(0)S(0)S(0)LLT(-17)S(-26)LPS(-38)IAK
		S	741	LAAASYWKPQS(0.331)S(0.331)S(0.331)LLT(0.007)S(0.001)LPSIAK	LAAAS(-58)Y(-71)WKPQS(0)S(0)S(0)LLT(-17)S(-26)LPS(-38)IAK
		S	757	FHDPGS(0.489)AT(0.489)IVS(0.02)LHMS(0.001)PLT(0.001)R	FHDPGS(0)AT(0)IVS(-14)LHMS(-27)PLT(-27)R
		T	759	FHDPGS(0.489)AT(0.489)IVS(0.02)LHMS(0.001)PLT(0.001)R	FHDPGS(0)AT(0)IVS(-14)LHMS(-27)PLT(-27)R

Amino acid	Positions within proteins	+ RSK1 replicate1			+ RSK1 replicate2			+ RSK1 replicate3		
		Localization prob + RSK1_rep1	PEP + RSK1_rep1	Score + RSK1_rep1	Localization prob + RSK1_rep1	PEP + RSK1_rep1	Score + RSK1_rep1	Localization prob + RSK1_rep1	PEP + RSK1_rep1	Score + RSK1_rep1
S	739	0.319979	1.43371E-07	108.57	0.330704	1.14206E-12	139	0.317912	4.54302E-05	82.8
S	740	0.319979	1.43371E-07	108.57	0.330704	1.14206E-12	139	0.317912	4.54302E-05	82.8
S	741	0.319979	1.43371E-07	108.57	0.330704	1.14206E-12	139	0.317912	4.54302E-05	82.8
S	757	0.489112	0.0105481	46.621	0.350352	0.0108331	46.178			
T	759	0.489112	0.0105481	46.621	0.350352	0.0108331	46.178			

Amino acid	Positions within proteins	no RSK1 replicate1			no RSK1 replicate2			no RSK1 replicat3		
		Localization prob no RSK1_rep1	PEP no RSK1_rep1	Score no RSK1_rep1	Localization prob no RSK1_rep1	PEP no RSK1_rep1	Score no RSK1_rep1	Localization prob no RSK1_rep1	PEP no RSK1_rep1	Score no RSK1_rep1
S	739									
S	740									
S	741									
S	757	0		NaN	0		NaN			
T	759	0		NaN	0		NaN			

Amino acid	Positions within proteins	Position in peptide	Charge	Mass error [ppm]	Localization prob	Score diff	PEP	Score	Delta score	Score for localization
S	739	11	3	1.0308	0.330704	0	1.14206E-12	139	127.69	139
S	740	12	3	1.0308	0.330704	0	1.14206E-12	139	127.69	139
S	741	13	3	1.0308	0.330704	0	1.14206E-12	139	127.69	139
S	757	6	3	0.56203	0.489112	0	0.0105481	46.621	40.187	46.621
T	759	8	3	0.56203	0.489112	0	0.0105481	46.621	40.187	46.621

Table S3. Phosphosites RAPTOR1B, related to Figure 2.

Parameter	Value
Version	1.6.10.43
Include contaminants	FALSE
PSM FDR	0.01
PSM FDR Crosslink	0.01
Protein FDR	0.01
Site FDR	0.01
Use Normalized Ratios For Occupancy	TRUE
Min. peptide Length	7
Min. score for unmodified peptides	0
Min. score for modified peptides	40
Min. delta score for unmodified peptides	0
Min. delta score for modified peptides	6
Min. unique peptides	1
Min. razor peptides	1
Min. peptides	1
Use only unmodified peptides and	TRUE
Modifications included in protein quantification	Oxidation (M);Acetyl (Protein N-term);Phospho (STY)
Peptides used for protein quantification	Unique
Discard unmodified counterpart peptides	TRUE
Label min. ratio count	1
Use delta score	FALSE
iBAQ	TRUE
iBAQ log fit	TRUE
Match between runs	TRUE
Matching time window [min]	0.7
Match ion mobility window [indices]	0.05
Alignment time window [min]	20
Alignment ion mobility window [indices]	1
Find dependent peptides	FALSE
Fasta file	Z:\GEJAE\MaxQuant\databases\Araport11plus_DE20191003.fasta
Decoy mode	revert
Include contaminants	FALSE
Advanced ratios	TRUE
Fixed andromeda index folder	Z:\GEJAE\MaxQuant\Andromeda\Andromeda_index
Temporary folder	Z:\GEJAE\MaxQuant\MQ_TEMP
Combined folder location	Z:\GEJAE\PSB-295_GEJAE
Second peptides	TRUE
Stabilize large LFQ ratios	TRUE
Separate LFQ in parameter groups	FALSE
Require MS/MS for LFQ comparisons	TRUE
Calculate peak properties	FALSE
Main search max. combinations	200
Advanced site intensities	TRUE
Write msScans table	FALSE
Write msmsScans table	FALSE

Write ms3Scans table	FALSE
Write allPeptides table	FALSE
Write mzRange table	FALSE
Write pasefMsmsScans table	FALSE
Write accumulatedPasefMsmsScans table	FALSE
Max. peptide mass [Da]	4600
Min. peptide length for unspecific search	8
Max. peptide length for unspecific search	25
Razor protein FDR	TRUE
Disable MD5	FALSE
Max mods in site table	3
Match unidentified features	FALSE
Epsilon score for mutations	Z:\GEJAE\PSB-295_GEJAE
Evaluate variant peptides separately	TRUE
Variation mode	None
MS/MS tol. (FTMS)	20 ppm
Top MS/MS peaks per Da interval. (FTMS)	12
Da interval. (FTMS)	100
MS/MS deisotoping (FTMS)	TRUE
MS/MS deisotoping tolerance (FTMS)	7
MS/MS deisotoping tolerance unit (FTMS)	ppm
MS/MS higher charges (FTMS)	TRUE
MS/MS water loss (FTMS)	TRUE
MS/MS ammonia loss (FTMS)	TRUE
MS/MS dependent losses (FTMS)	TRUE
MS/MS recalibration (FTMS)	FALSE
MS/MS tol. (ITMS)	0.5 Da
Top MS/MS peaks per Da interval. (ITMS)	8
Da interval. (ITMS)	100
MS/MS deisotoping (ITMS)	FALSE
MS/MS deisotoping tolerance (ITMS)	0.15
MS/MS deisotoping tolerance unit (ITMS)	Da
MS/MS higher charges (ITMS)	TRUE
MS/MS water loss (ITMS)	TRUE
MS/MS ammonia loss (ITMS)	TRUE
MS/MS dependent losses (ITMS)	TRUE
MS/MS recalibration (ITMS)	FALSE
MS/MS tol. (TOF)	40 ppm
Top MS/MS peaks per Da interval. (TOF)	10
Da interval. (TOF)	100
MS/MS deisotoping (TOF)	TRUE
MS/MS deisotoping tolerance (TOF)	0.01
MS/MS deisotoping tolerance unit (TOF)	Da
MS/MS higher charges (TOF)	TRUE
MS/MS water loss (TOF)	TRUE
MS/MS ammonia loss (TOF)	TRUE
MS/MS dependent losses (TOF)	TRUE
MS/MS recalibration (TOF)	FALSE
MS/MS tol. (Unknown)	20 ppm

Top MS/MS peaks per Da interval. (Unknown)	12
Da interval. (Unknown)	100
MS/MS deisotoping (Unknown)	TRUE
MS/MS deisotoping tolerance (Unknown)	7
MS/MS deisotoping tolerance unit (Unknown)	ppm
MS/MS higher charges (Unknown)	TRUE
MS/MS water loss (Unknown)	TRUE
MS/MS ammonia loss (Unknown)	TRUE
MS/MS dependent losses (Unknown)	TRUE
MS/MS recalibration (Unknown)	FALSE
Site tables	Oxidation (M)Sites.txt;Phospho (STY)Sites.txt

Table S4. MaxQuant search parameters, related to Figure 2.

Table S1

Click here to access/download

Supplemental Videos and Spreadsheets

Table S1.xlsx